Synthesis and Characterization of Radical Cations Derived from Mono- and Biferrocenyl-Substituted 2-Aza-1,3-butadienes: A Study of the Influence of an Asymmetric and Oxidizable Bridge on Intramolecular Electron Transfer

Vega Lloveras,[a] Antonio Caballero,[b] Alberto Tárraga,[b] M. Desamparados Velasco,[b] Arturo Espinosa,[b] Klaus Wurst,[c] David J. Evans,[d] José Vidal-Gancedo,[a] Concepció Rovira,[a] Pedro Molina,*[b] and Jaume Veciana*[a]

Keywords: Charge transfer / Electrochemistry / Electron transfer / Metallocenes / Optical spectroscopy

The synthesis and study of structural and electronic properties of mono-ferrocenyl π-conjugated complexes **5a**–**d**, whose electronic characteristics have been systematically varied by introducing an electron-donating or electron-withdrawing substituent either at the 1-position or at the 4-position of the 2-aza-1,3-butadiene moiety linked to the ferrocenyl unit, are presented. The structural and electronic properties of the homobimetallic complex **5f**, with two ferrocene units linked through the asymmetric and oxidizable 2-aza-1,3-butadiene bridge, is also reported. The crystal structures of complexes **5b**, **5d**, and **5f** show a large degree of conjugation in this family of compounds. Complexes **5** show a rich electrochemical behavior due both to the oxidation of ferrocenyl units and the 2-aza-1,3-butadiene bridge, as revealed by cyclic voltammetry. Radical cations $\mathbf{5}^{+\cdot}$ were prepared from **5** by coulometric oxidations following their generation by absorption spectroscopy. The electronic properties of all reported neutral and oxidized π-conjugated complexes have been investigated by means of UV/Vis–near-IR, EPR and ^{57}Fe Mössbauer spectroscopy. The detailed study of mono-oxidized species $\mathbf{5a}^{+\cdot}$–$\mathbf{5f}^{+\cdot}$ has permitted the determination of the influence of an asymmetric bridge with an electroactive character on the intramolecular electron transfer (IET) phenomenon, thus demonstrating that the 2-aza-1,3-butadiene bridge promotes the IET between the two metallic units of $\mathbf{5f}^{+\cdot}$ through two different pathways. The experimental data and conclusions are supported by DFT computations (B3LYP/3-21G*) and time-dependent DFT methods.
(© Wiley-VCH Verlag GmbH & Co. KGaA, 69451 Weinheim, Germany, 2005)

Introduction

Currently, there is considerable interest in the study of the properties of compounds bearing multiple redox centers separated by an organic bridge and, in particular, those that are able to produce mixed-valence species.[1] Such species are interesting not only because of their importance in producing new valuable materials, such as molecular wires and switches, that show intramolecular electron transfer (IET) phenomena, but also to understand the role of biologically relevant mixed-valence compounds.[2] One of the richer areas of metallocene chemistry is the study of general strategies for assembling two or more such electroactive metal fragments in close proximity in order to determine the type of electronic interactions between the metal fragments.[3] Among the various possibilities to bridge two cyclopentadienyl-type (Cp) ligands, emphasis has been laid on the electronic and steric properties of organic bridges because both will influence the interaction between the metal fragments bound to the Cp's and, in many cases, these factors will not be independent.

It is worth noting that IET can be monitored by the study of optical transitions occurring in mixed-valence complexes,[4] and that intervalence charge-transfer (IV-CT) bands may be observed in both σ- and π-bridged systems. In the former case, a through-space mechanism is generally believed to be responsible, such that low-energy bands at the near-IR are usually only observed in species that are sufficiently flexible to allow the two metal centers to come into close proximity. In π-bridged systems, near-IR bands are much more widely observed, even when the metals are well separated by rigid bridges, thereby suggesting that through-bond mechanisms are involved. IET in such π-bridged systems may proceed either by a superexchange and/or a hopping mechanism.[5] In the superexchange

[a] Institut de Ciència de Materials de Barcelona (CSIC), Campus Universitari de Bellaterra,
08193, Cerdanyola, Spain
Fax: +34-93-580-5729
E-mail: vecianaj@icmab.es
[b] Universidad de Murcia, Departamento de Química Orgánica, Facultad de Química,
Campus de Espinardo, 30100 Murcia, Spain
Fax: +34-968-364149
E-mail: pmolina@um.es
[c] Institut für Allgemeine Anorganische und Theoretische Chemie, Universität Innsbrück,
6020, Innrain 52a, Innsbruck, Austria
[d] Department of Biological Chemistry, John Innes Centre, Norwich Research Park, Colney, Norwich, NR4 7UH, UK
Supporting information for this article is available on the WWW under http://www.eujic.org/ or from the author.

 © 2005 Wiley-VCH Verlag GmbH & Co. KGaA, Weinheim **DOI: 10.1002/ejic.200400992**

mechanism the bridge serves solely to mediate the wavefunctions of the two electroactive centers that act as electron-donor and -acceptor groups; the electron (or hole) is never vibronically localized on the bridge. In contrast, in the hopping mechanism the electron (or hole) is located at the bridge for a short time (vibronically localized) during its journey from one redox center to the other. The former mechanism is generally the origin of many of the observed IV-CT bands in mixed-valence species, while the hopping one is much less common, probably because of the strict structural and electronic requirements that must be fulfilled by the bridge. Nowadays there is a great interest in the development of organic bridges that favor the hopping mechanism between the two electroactive centers since they could provide new molecular devices that act as electronic relays to promote IETs over large distances.

A large number of bis-metallocenes and metallocenes linked by saturated carbon bridges have been synthesized and studied with respect to metal–metal interactions. It has been demonstrated that, compared to bis-metallocenes, species linked by a single carbon bridge show substantially weaker metal–metal interactions.[6] In general, stronger electrochemical metal–metal interactions occur when two linkages are made between two metallocenes and the metals are brought into closer proximity. On the other hand, IV-CT absorptions are usually not observed in the mono-oxidized derivatives of ferrocenes with insulating hydrocarbon bridges.[7] Most bis-metallocenes linked by saturated carbon bridges belong to class I in the Robin–Day classification,[8] the only interaction detected being at the electrochemical level and which can be attributed only to electrostatic and inductive effects. In contrast, ferrocenyl groups linked by unsaturated bridges show slightly larger metal–metal interactions than those with analogous saturated bridges,[2c,9–13] and the corresponding mono-oxidized olefin-bridged species show IV-CT absorptions in the near-IR region. Thus, many such species belong to class II, in which there is a moderate coupling between the two electroactive centers mediated by the organic bridge through a superexchange mechanism. Intermetallic interactions of different magnitudes have been observed in diferrocene complexes in which the two metallocene units are linked through a symmetric spacer with two conjugated double bonds (e.g. butadiene,[14] 1,4-diaza-1,3-butadiene,[15] 2,3-diaza-1,3-butadiene,[16] and others[17]). However, no examples have been reported of metal–metal interactions between metallocene units linked by an asymmetric spacer like the 2-aza-1,3-butadiene bridge.

Here we wish to present the synthesis and study of structural and electronic properties of ferrocenyl (Fc) π-conjugated complexes **5a**–**d**, whose electronic properties have been systematically varied by introducing an electron-donating or electron-withdrawing substituent, either at the 1-position or at the 4-position of the 2-aza-1,3-butadiene moiety linked to the ferrocenyl unit. We also wish to present here a study of the homobimetallic complex **5f**, which contains two ferrocene units linked by the asymmetric 2-aza-1,3-butadiene bridge. The mono-oxidized species of this complex, $\mathbf{5f}^{+\bullet}$, has permitted the study of the influence of an asymmetric bridge with an electroactive character on the intramolecular electron transfer (IET) phenomenon, demonstrating that the 2-aza-1,3-butadiene bridge favors the IET between the two metallic centers.

Results and Discussion

Synthesis and Characterization

Compounds **5** were all prepared from the readily available diethyl aminomethylphosphonate (**1**),[18] which was condensed with the appropriate aromatic or organometallic aldehyde **2** to give the corresponding *N*-substituted diethyl aminomethylphosphonate **3** in excellent yields (85–95%). Generation of the metalloenamine by treatment with *n*BuLi at –78 °C and subsequently with one equivalent of the aldehyde **4** provided the 1,4-disubstituted 2-aza-1,3-butadienes **5** in yields ranging from 40% to 90% (Scheme 1). While two individual operations are required in the latter synthesis, it is possible to execute the entire sequence of reactions in a single flask without isolation of the intermediates **3** without affecting the yield. However, in this case, isolation of compounds **5** proved to be more difficult. Compounds **5**, recrystallized from dichloromethane/diethyl ether (1:10), were characterized by mass spectroscopy and ^{1}H and ^{13}C NMR spectroscopy, as well as by elemental analyses.

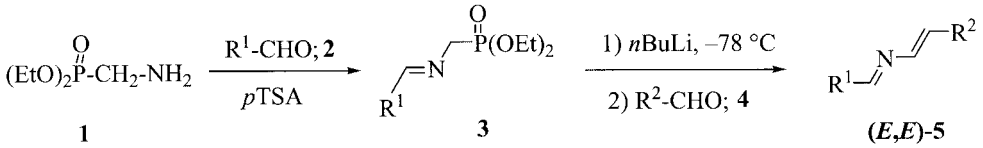

	R^1
3a	4-H_3CO-C_6H_4
3b	4-O_2N-C_6H_4
3c	Fc

	R^1	R^2
5a	4-H_3CO-C_6H_4	Fc
5b	4-O_2N-C_6H_4	Fc
5c	Fc	4-H_3CO-C_6H_4
5d	Fc	4-O_2N-C_6H_4
5e	4-H_3CO-C_6H_4	4-H_3CO-C_6H_4
5f	Fc	Fc

Scheme 1.

 © 2005 Wiley-VCH Verlag GmbH & Co. KGaA, Weinheim

Assignment of the configuration of the double bonds present in the 1,4-disubstituted 2-aza-1,3-butadienes **5** was achieved by inspection of the ^{1}H NMR spectroscopic data. It is well established that the condensation reaction between a primary amine and an aldehyde is not stereoselective, hence both (*E*)- and (*Z*)-aldimine isomers are generally present in the reaction product. However, it must be emphasized that the condensation reaction between **1** and the appropriate aldehyde **2** takes place stereoselectively to give exclusively the (*E*)-isomer, as ascertained by ^{1}H NMR spectroscopy. Indeed, an NOE effect is observed to the methylene group on irradiation of the aldiminic proton of **3a**. On the other hand, *N*-substituted diethyl aminophosphonates **3**, after deprotonation with *n*BuLi, react smoothly in THF with the corresponding aldehyde **4** to give only the *trans* configured carbon-carbon double bond, as is expected in a Horner–Wadsworth–Emmons olefination process. This configuration was confirmed by the characteristic vicinal coupling constants (J = 14.0 Hz) in the ^{1}H NMR spectrum. In addition, NOE and two-dimensional NOESY experiments on a solution of compound **5f** in $CDCl_3$ confirmed not only the (*E*,*E*)-configuration of the double bonds present in the bridge, but also the *s-cis*-conformation in this solvent. Thus, on irradiation at δ = 7.04 ppm (H_4) an NOE effect is observed on the aldiminic H_1; no NOE effect is observed to H_1 when irradiation takes place at δ = 6.63 ppm (H_3).

X-ray Crystal Structures

Single crystals of compounds **5b**, **5d**, and **5f**, suitable for X-ray structure determination, were grown from diffusion of *n*-hexane into a solution of the compound in CH_2Cl_2. The crystal data and details of data collection and structure refinement are given as Supporting Information (Table S1). Attempts to grow good-quality single crystals of **5a** and **5c** for X-ray determination were unsuccessful.

Compound **5b** crystallizes in the triclinic space group $P\bar{1}$ with four molecules in the unit cell. Two independent molecules were found per asymmetric unit. Figure 1 (see a) shows the ORTEP drawing of the molecular structure of **5b** with the atomic numbering scheme. The molecular structure reveals that **5b** is present as the (*E*,*E*)-isomer, as is observed in solution by ^{1}H NMR spectroscopy, and has an *s-trans* configuration in the solid state. The interatomic distances and bond angles of **5b** are close to those previously observed for ferrocene[19] and other substituted ferrocene

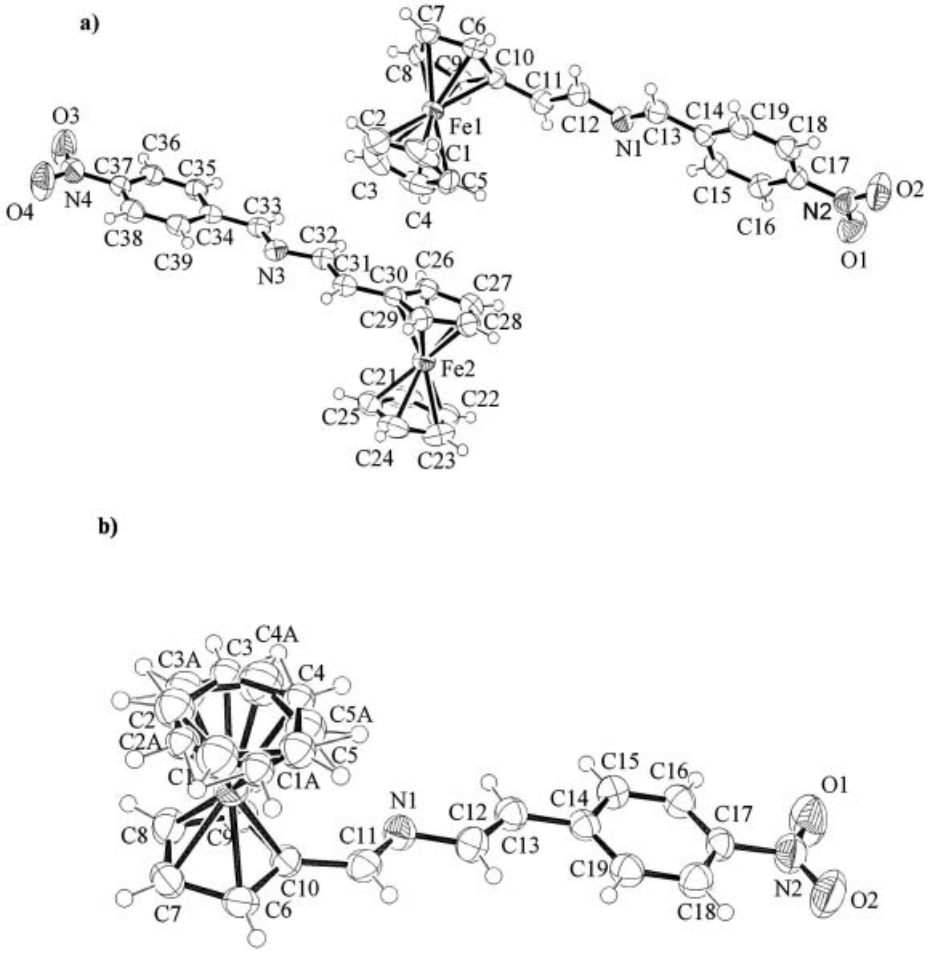

Figure 1. ORTEP views of the asymmetric unit of **5b** showing the atom numbering scheme (a) and of **5d** showing the atom numbering scheme (b). Thermal ellipsoids are drawn at the 50% probability level.

 © 2005 Wiley-VCH Verlag GmbH & Co. KGaA, Weinheim

compounds.[20] The most interesting structural feature of **5b** is that all atoms of the 2-aza-1,3-butadiene bridge and the two attached rings are disposed in a planar configuration, thus indicating a large degree of π-conjugation and rigidity of this organic ligand.

Compound **5d** crystallizes in the monoclinic space group *P*21/*n* with four molecules in the unit cell. Figure 1 (see b) shows the ORTEP drawing with the atomic numbering scheme. Molecules of this compound are also present as the (*E*,*E*)-isomer, as observed in solution by ^{1}H NMR spectroscopy, and have an *s-trans* configuration in the solid state. The bond and dihedral angles reveal that all the atoms of the bridge and the two linked rings are disposed in a planar configuration, as in compound **5b**, thus indicating a large degree of conjugation in the π-system.

Compound **5f** crystallizes in the monoclinic space group *P*21/*c* with two molecules in the unit cell. Figure 2 shows the ORTEP drawing of **5f** with the atomic numbering scheme. The molecular structure of **5f** reveals a 1:1 disorder of the two atoms C12 and N1 at the same position. The crystallographic asymmetric unit is only one half of the molecule, since the other half is generated by a symmetry operation with a center of symmetry, as shown in Figure 2. Since the molecule does not really possess a symmetry center it must be disordered, therefore C12 and N1 were refined each with an occupancy of 0.5 with the same coordinates and temperature factors. Molecules of **5f** are also present as the (*E*,*E*)-isomer, as observed in solution by ^{1}H NMR spectroscopy, but in the solid state they adopt an *s-trans* conformation in contrast to the major conformation adopted in solution (vide supra). One of the two equivalent possibilities of the molecule is shown in Figure 2.

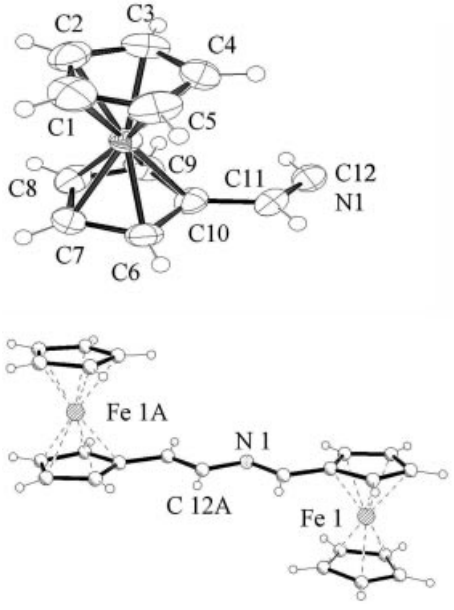

Figure 2. Top: ORTEP view of the asymmetric unit of **5f** showing the atom numbering scheme. Thermal ellipsoids are drawn at the 50% probability level. Bottom: drawing of a complete molecule of **5f**.

Theoretical Calculations

Geometry optimizations at the DFT level were carried out for neutral 2-aza-1,3-butadienes **5** as well as for the oxidized species **5**$^{\bullet+}$; the resulting geometrical parameters are gathered in Table 1. For those compounds whose X-ray structures are reported here, a high degree of coincidence is observed with the calculated values, as shown by the following critical geometrical parameters: the calculated N(bridge)···Fe distances for **5b**, **5d**, and **5f** are 5.309, 3.868, and 3.885 (Fe_1) and 5.380 Å (Fe_4), while the corresponding experimental distances are 5.242, 3.893, and 3.967 and 5.169 Å, respectively; the calculated Fe_1···Fe_4 distance in **5f** is 9.225 Å, while the experimental one is 9.107 Å. The other two calculated structures **5a** and **5c** display similar values (5.350 and 3.860 Å, respectively) for the N(bridge)···Fe distance. On the other hand, all calculated structures have a pure *s-trans* conformation (C1–N2–C3–C4 dihedral angles of 179.7°, 178.3°, 177.5°, 178.6°, and 179.2° for **5a**–**d** and **5f**, respectively), with the substituted phenyl rings almost parallel to the 2-aza-1,3-butadiene plane (angles between mean planes of 0.3°, 3.5°, 4.7°, and 1.4° for **5a**–**d**, respectively) and the bridge-attached Cp rings with small twisting angles (13.6°, 5.6°, 7.8°, 3.5°, 1.4°, and 12.1° for **5a**–**d** and Fc_1 and Fc_4 in **5f**, respectively). Where available, all experimental ring (Cp or substituted phenyl) twisting angles are systematically higher than the corresponding calculated values. From these calculations it is possible to conclude that both neutral 2-aza-1,3-butadienes **5** and oxidized species **5**$^{\bullet+}$ show planar structures exhibiting a large conjugation and a high structural rigidity (Table 1).

Electronic Spectroscopy

The UV/Visible data obtained in CH_2Cl_2 for **5a**–**d** and **5f** are collected in Table 2. These spectra are characterized by a very strong absorption with a maximum between 336 and 375 nm, which is assigned to a localized π-π* excitation mainly within the 2-aza-1,3-butadiene bridge. In addition to this band, another weaker absorption is visible between 469 and 535 nm, which is assigned to another localized excitation with a lower energy produced either by two nearly degenerate transitions, an Fe^{II} d-d transition[21] (e.g. HOMO–1 → LUMO+3 in **5a**), or by a metal-to-ligand charge transfer (MLCT) process (d_π-π*)[22] (e.g. HOMO–3 → LUMO+1 in **5a**). By comparison of the compounds with the ferrocenyl unit in the same position of the bridge it is easy to conclude that the presence of an electron-donating methoxy group (**5a** and **5c**) results in a significant decrease of the wavelength of the absorption maximum relative to the compounds with a nitro substituent (**5b** and **5d**). On the other hand, the compounds with the ferrocenyl group at the 4-position of the bridge show a shift of the absorption maxima to longer wavelengths relative to the compounds with the ferrocenyl group at the 1-position. Therefore, the calculated energy gap between HOMO and LUMO in the first position (3.6558 and 2.8194 eV for **5a** and **5b**, respectively) is slightly smaller than in the second position (3.6889 and

 © 2005 Wiley-VCH Verlag GmbH & Co. KGaA, Weinheim

Table 1. Selected calculated[a] and geometrical parameters[b] for neutral 2-aza-1,3-butadienes **5** and oxidized species $\mathbf{5}^{+\cdot}$.

	R^1–C^1	C^1–N^1	N^2–N^3	C^3–C^4	C^4–R^4	$C^1N^2C^3$	$C^1N^2C^3C^4$	$R^{1\#}Azd^{\#}$	$Azd^{\#}R^{4\#}$	$Fe^1\cdots N^2$	$Fe^4\cdots N^2$	$Fe^1\cdots Fe^4$
5a	1.457	1.294	1.399	1.348	1.447	119.8	179.7	0.3	13.6		5.350	
5b	1.462	1.293	1.395	1.350	1.443	120.6	178.3	3.5	5.6		5.309	
	(1.454)	(1.280)	(1.387)	(1.335)	(1.447)	(117.7)	(176.7)	(5.2)	(9.6)		(5.242)	
5c	1.444	1.294	1.401	1.348	1.459	119.5	177.5	7.8	4.7	3.860		
5d	1.439	1.297	1.398	1.349	1.458	119.0	178.6	3.5	1.4	3.868		
	(1.442)	(1.282)	(1.394)	(1.320)	(1.460)	(117.1)	(179.2)	(3.9)	(4.2)	(3.893)		
5f	1.439	1.297	1.398	1.349	1.458	119.0	178.6	1.4	12.1	3.885	5.380	9.225
	(1.442)	(1.282)	(1.394)	(1.320)	(1.460)	(117.1)	(179.2)	(8.1)	(8.1)	(3.967)	(5.169)	(9.107)
$\mathbf{5a}^{+\cdot}$	1.431	1.313	1.370	1.366	1.424	119.5	177.5	1.0	7.4		5.445	
	(–0.026)	(+0.019)	(–0.029)	(+0.018)	(–0.023)	(–0.3)	(–2.2)	(+0.7)	(–6.2)		(+0.095)	
$\mathbf{5c}^{+\cdot}$	1.433	1.308	1.374	1.367	1.436	121.3	178.3	4.2	2.1	3.984		
	(–0.011)	(+0.014)	(–0.027)	(+0.019)	(–0.023)	(+1.8)	(+0.8)	(–3.6)	(–2.6)	(+0.124)		
$\mathbf{5d}^{+\cdot}$	1.446	1.296	1.392	1.354	1.455	121.0	179.9	7.6	1.0	3.900		
	(+0.007)	(–0.001)	(–0.006)	(+0.005)	(–0.003)	(+2.0)	(+1.3)	(+4.1)	(–0.4)	(+0.032)		
$\mathbf{5f}^{+\cdot}$	1.420	1.314	1.373	1.364	1.425	118.8	176.1	3.4	9.0	3.842	5.456	9.261
	(–0.024)	(+0.020)	(–0.028)	(+0.017)	(–0.022)	(–0.8)	(–3.1)	(+2.0)	(–1.6)	(–0.043)	(+0.076)	(+0.036)
$\mathbf{5f}^{2+}$	1.412	1.409	1.295	1.458	1.415	119.3	178.1	24.5[c]	35.7[c]	3.057	4.124	7.172
	(–0.008)	(+0.094)	(–0.078)	(+0.094)	(–0.010)	(+0.5)	(–0.2)	(+21.1)	(+26.7)	(–0.785)	(–1.332)	(–2.089)

[a] The experimental values for neutral compounds, where available, and, for oxidized species, the calculated absolute difference in relation to the precedent structure before one-electron oxidation, are given in parentheses. [b] Distances [Å] and bond and dihedral angles [°]; # stands for the azadiene skeleton (Azd), Cp or substituted-phenyl mean planes. [c] Unusually large angles between mean planes do not reflect a twisting rotation around a C_{Cp}–C_{Azd} bond, but a bending distortion of the exocyclic substituent towards Fe atom in order to alleviate the electron deficiency. See for instance ref.[49]

Table 2. Calculated and experimental electronic absorption bands of neutral compounds **5a**–**d** and **5f**.

Compound	R^1	R^2	Calculated λ_{max} [nm] (oscillator strength)	Experimental[a] λ_{max} [nm] (10^{-3} ε, $M^{-1}cm^{-1}$)
5a	4-$CH_3OC_6H_4$	Fc	343.6 (0.7961), 375.8 (0.1944), 469.7 (0.0052)	345 (24.5), 360 (sh), 470 (2.1)
5b	4-$NO_2C_6H_4$	Fc	378.7 (0.4862), 526.9 (0.0965)	375 (16.9), 535 (4.4)
5c	Fc	4-$CH_3OC_6H_4$	341.3 (1.2479), 369.2 (0.0132), 470.3 (0.0033)	342 (20.7), 356 (sh), 469 (1.9)
5d	Fc	4-$NO_2C_6H_4$	366.1 (0.5466), 522.6 (0.0690)	371 (18.7), 504 (4.5)
5f	Fc	Fc	336.2 (0.0415), 339.9 (0.1006), 476.2 (0.0033)	336 (25.5), 346 (sh), 478 (3.6)

[a] In CH_2Cl_2.

2.9889 eV for **5c** and **5d**, respectively) and this gap is greatly increased by the presence of an electron-donating substituent at the aromatic ring. Finally, the homobimetallic complex **5f** shows an absorption spectrum that is very similar to those of complexes **5a** and **5c**, as expected from the similar electron-donor abilities of ferrocenyl and *p*-methoxyphenyl groups (calculated HOMO–LUMO gap of 3.7785 eV for **5f**).

At this point, it is useful to consider the electronic transitions in terms of the molecular orbitals involved. Analysis of the electronic transitions by time-dependent DFT methods (TDDFT) gave essentially identical results for each studied compound between experimental and calculated transitions (summarized in Table 2). The agreement between calculated optical transitions and the experimentally observed results lends credence to the used theoretical level as well as to the attained geometries and the molecular-orbital model developed to explain such optical transitions. In addition, such an agreement confirms the assignation previously made to each optical transition.

Electrochemistry

Compounds **5** are all expected to show electroactivity due both to the Fe^{II}/Fe^{III} couple and the oxidation of the 2-aza-1,3-butadiene bridge. Indeed, monoferrocenyl derivatives **5a**–**d** show two oxidation waves in the range 0–1.5 V vs. SCE; their potentials are collected in Table 3. The first oxidation wave for all compounds is reversible and occurs at potentials close to that of the Fe^{II}/Fe^{III} couple in ferrocene (0.460 V vs. SCE, or 0.530 V vs. decamethylferrocene, DMFc).[23] Therefore, this wave is assigned to the Fe^{II}/Fe^{III} redox couple. The oxidation potentials of the ferrocenyl units of these compounds show a dependence on the position of the 2-aza-1,3-butadiene bridge to which they are attached and also on the electron-donating ability of the aromatic group linked to the bridge. Thus, higher potentials are observed when the ferrocenyl is attached at the 1-position of the bridge and when the substituent of the aromatic ring is a nitro group. In contrast to the first oxidation wave, the second wave is clearly not reversible for **5a**–**c** under the conditions of our experiments, since only the anionic peak appears in the cyclic voltammogram. Taking into account that the *p*-methoxyphenyl moiety is the most "ferrocene-like" group in terms of its electron-donating capability, as demonstrated experimentally by the similarity of the UV/Vis spectra of **5a**, **5c**, and **5f** (vide supra), and also by independent non-linear optical measurements,[24] the 1,4-bis(*p*-methoxyphenyl)-2-aza-1,3-butadiene **5e** was also studied for comparison purposes. The CV of this compound shows two

 © 2005 Wiley-VCH Verlag GmbH & Co. KGaA, Weinheim

irreversible oxidation waves at 1.084 and 1.440 V vs. DMFc that may be assigned to the oxidation of the N atom of the bridge and the *p*-methoxyphenyl group, respectively. This assignment is based on the fact that when the N atom of **5e** is protonated under acidic conditions the first oxidation peak disappears while the second remains unchanged. On the basis of these observations, the second wave observed in the CVs of compounds **5a**–**c** is also assigned to the oxidation of the 2-aza-1,3-butadiene group, the potential of which varies from 1.090 V to 1.416 V vs. DMFc and also shows a dependence on the substituents of the aromatic ring and on the relative position of the ferrocenyl and aromatic groups. Such an irreversible oxidation wave is not observed for compound **5d**, probably because it appears at a potential more positive than +1.5 V vs. DMFc due to the strong electron-withdrawing character of the nitro group.

Table 3. Cyclic voltammogram data for compounds **5a**–**f** in CH_2Cl_2.

Compound	R^1	R^2	$^1E_{1/2}$ (Fc^+/Fc)[a]	$^2E_{ap}$ (irrev)[a]
5a	4-$CH_3OC_6H_4$	Fc	0.530	1.090
5b	4-$NO_2C_6H_4$	Fc	0.590	1.190
5c	Fc	4-$CH_3OC_6H_4$	0.698	1.416
5d	Fc	4-$NO_2C_6H_4$	0.704	–
5e	4-$CH_3OC_6H_4$	4-$CH_3OC_6H_4$	–	1.084, 1.440
5f	Fc	Fc	0.560 0.770	1.116

[a] $E_{1/2}$ [V] vs. decamethylferrocene.

To gain further insight into the nature of the irreversible oxidation wave, the electrochemical behavior of compounds **5a**–**d** was investigated in the presence of HBF_4. Upon protonation, the potential shift of the ferrocenyl unit present in these compounds was found to be strongly dependent on its position in the 2-aza-1,3-butadiene bridge. When it is placed at the 4-position a $\Delta E_{1/2}$ (L – LH^+) of 70 mV (**5a**) and 80 mV (**5b**) was observed, while when it is placed at the 1-position the corresponding shifts are 300 mV (**5c**) and 320 mV (**5d**). Additionally, in all these cases, the irreversible wave associated with the oxidation of the bridge disappeared upon protonation, except for **5c**, which seems to be due to the oxidation of the methoxy group present in the ring.

The species formed during the irreversible oxidation waves of **5a**–**c** are probably the radical cations centered mainly at the N atom of the 2-aza-1,3-butadiene bridge, species which must be relatively unstable under the experimental conditions used. Although no electrochemical oxidation study of the 2-aza-1,3-butadiene fragment has been reported, this description is based on the fact that the anodic oxidation of the closely related *N*-benzylidene-*p*-anisidine Schiff bases show two irreversible anodic peaks at 1.08–1.25 and 1.41–1.61 V vs. SCE. The peak potentials of the first wave, which show good linearity against the σ^+ values of the substituent in the benzylidene ring, are ascribed to the formation of a radical cation centered at the nitrogen atom, whereas the second peak is attributed to the oxidation of the substituent in the aromatic ring.[25] In this sense, the electrochemical behaviors of compound **5e** and *N*-*p*-methoxybenzylidene-*p*-anisidine are almost identical, since the CV displays two irreversible oxidation peaks at 1.08 and 1.52 V vs. SCE.

The CV of **5f**, which contains two ferrocenyl groups, was recorded in two different experiments. Firstly, the CV (see a in Figure 3) scanned from 0–1 V shows two closely spaced reversible one-electron oxidations corresponding to the oxidation of the ferrocenyl units present in the molecule. Secondly, when the CV was run from 0.0–1.6 V, after the first scan, three oxidation waves were observed: two for the ferrocenyl units and one for the oxidation of the bridge. The cathodic return wave is, in general, higher and thinner than the anodic forward wave, which can be attributed to some adsorption of the oxidized compound onto the electrode surface in the ferrocenium form. The difference between the anodic and cathodic peak potentials (ΔE_p) is lower than the 58 mV value expected for a reversible single-electron wave of an electroactive species in solution at 20 °C (the fully adsorbed redox species would ideally have a ΔE_p value of zero). However, it is important to emphasize that the results obtained in the latter experiment could only be reproduced when the electrode was cleaned before subsequent scans were run. Otherwise, the wave corresponding to the oxidation of the bridge disappears, indicating that the electrode behaves as an insulator in the region in which the azadiene moiety is oxidized. The protonation process of **5f** was also followed by cyclic voltammetry. Upon protonation, the three waves present in the neutral ligand evolve into two waves in the protonated derivative, the latter wave appearing at almost the same potential region as that corresponding to the bridge in the neutral ligand. In order to understand the nature of the unit causing that wave, Osteryoung square-wave voltammetry (OSWV) experiments were carried out by protonation of **5f** (see b in Figure 3). While the neutral ligand exhibits only two oxidation waves at 0.560 and 0.770 V vs. DMFc, stepwise addition of HBF_4 resulted in a clear evolution of the first oxidation wave from 0.560 V to 0.630 V and the disappearance of the second oxidation wave, accompanied by concomitant appearance of a new oxidation wave at 1.060 V. The peak intensity of the new oxidation wave increases with the concentration of the acid added up to until two equivalents. At this point, the original oxidation waves disappear and the new ones reach full development. The resulting two oxidation waves, with a 1:1 ratio and a separation of 0.430 V, are due to the oxidation of the two ferrocenyl moieties in the protonated complex. Again, for reproducibility, it is very important to clean the electrode after each scan.

It is worth mentioning that the difference between the first two reversible oxidation waves in compound **5f** ($\Delta E_{1/2}$ = 210 mV) is much larger than those observed for most bis-ferrocenyl compounds with four-membered π-conjugated bridges, such as 1,4-bis(ferrocenyl)butadiene (129 mV),[14] 1,4-bis(ferrocenyl)butadiyne (120 mV),[10] 1,4-bis(ferrocenyl)-1,4-diazabutadiene (60 mV),[15] and 1,4-bis(ferrocenyl)-2,3-diaza-1,4-dimethylbutadiene (90 mV).[16] The origin of this large $\Delta E_{1/2}$ value must be ascribed to the asym-

 © 2005 Wiley-VCH Verlag GmbH & Co. KGaA, Weinheim

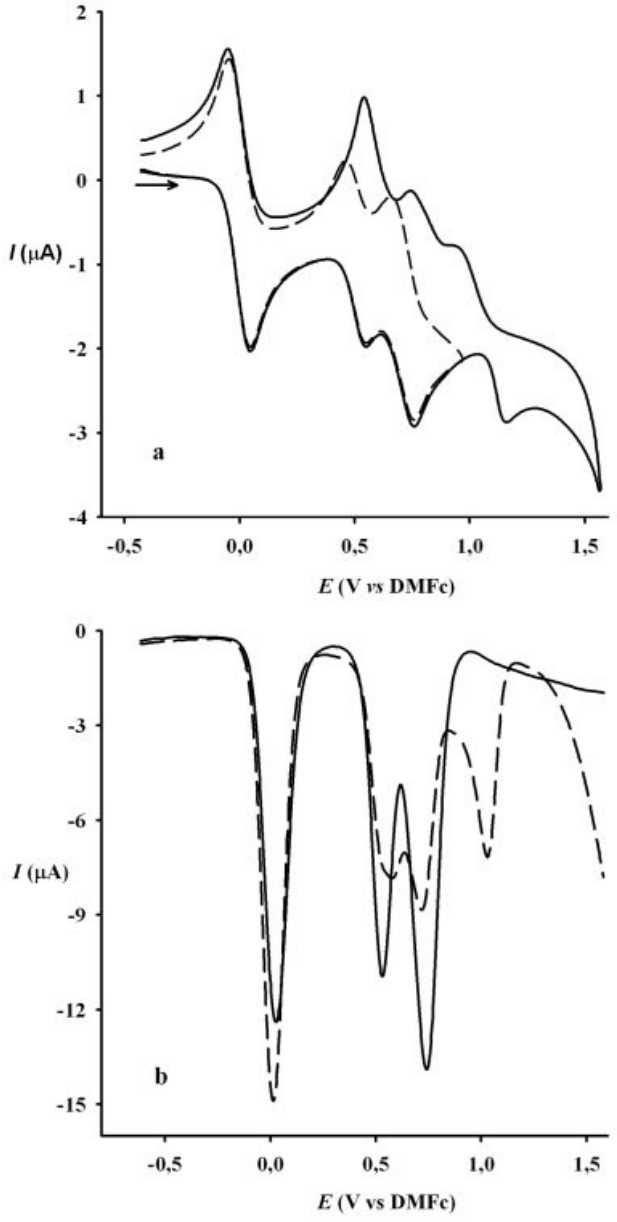

Figure 3. a) Cyclic voltammogram of compound **5f** (1 mM) in $CH_2Cl_2/[(nBu)_4N]ClO_4$ scanned at 0.1 $V s^{-1}$ from –0.5 V to 0.9 V (dash) and from –0.5 V to 1.6 V (solid). b) OSWV of compound **5f** (1 mM) in $CH_2Cl_2/[(nBu)_4N]ClO_4$ recorded at 0.1 $mV s^{-1}$ before (solid) and after (dash) addition of 1 equiv. of HBF_4. Decamethylferrocene (DMFc) was used as an internal standard.

metry of the bridge linking the two ferrocenyl groups. Thus, the distinct position of the N atom with respect to the two ferrocenyl groups should perturb the two ferrocenyl moieties to a different extent.

Optically Induced Intramolecular Electron Transfer in $5a^{\cdot+}$–$d^{\cdot+}$

It has been demonstrated that in electrochemically active ferrocenylthiophene derivatives, in which the gap between the metal and the organic bridge oxidation potentials is relatively small, it is possible, upon oxidation of the ferrocenyl group, to induce optically an electron transfer from the thienyl group to the Fe^{III} center.[26] This IET has an associated low-energy ligand-to-metal charge transfer (LMCT) band in the near-IR, which is very similar to those observed in symmetrical mixed-valence complexes. Moreover, it has been reported recently that the electrochemical oxidation of Fe^{II} centers of mono- or bis(ferrocenylethynyl)oligothiophenes, in which the potential difference between the reversible oxidation of the ferrocenyl group and the irreversible oxidation of the thienyl ring varies from 0.38 V to 1.12 V, yields the corresponding radical cations, which also exhibit oligothiophene-to-Fe^{III} charge-transfer LMCT bands in the near-IR region.[27] Taking into account that in compounds **5a**–**d** the potential differences between the two successive oxidation waves are in the range of 0.3–0.7 V (Table 3), and that these values are comparable to those of oligothiophene-substituted ferrocenes, the oxidized ferrocenyl derivatives $\mathbf{5a}^{\cdot+}$–$\mathbf{d}^{\cdot+}$ were considered suitable candidates to study the optically induced IET from the 2-aza-1,3-butadiene bridge to the Fe^{III} center. In favor of such an expectation is the recently reported fact that ferrocenyl derivatives containing a $-CH_2-N(R)-CH_2-$ bridge undergo intramolecular electron transfer between the Fe^{III} center and the nitrogen atom in the electrochemically oxidized state to give an intermediate containing an Fe^{II} center and a nitrogen with a radical cation character.[28]

The generation of the oxidized species derived from **5a**–**d** was performed electrochemically and monitored by absorption spectroscopy. Stepwise coulometric titrations were performed on ca. 2×10^{-3} M solutions of complexes **5a**–**d** in CH_2Cl_2, with $[(nBu)_4N]PF_6$ (0.15 M) as supporting electrolyte, and the absorption spectra were regularly recorded for different average number ($0 \le n \le 1$) of removed electrons. The UV/Vis–near-IR spectroscopic data of $\mathbf{5a}^{\cdot+}$–$\mathbf{d}^{\cdot+}$ are collected in Table 4. The spectra of $\mathbf{5a}^{\cdot+}$–$\mathbf{d}^{\cdot+}$ show three absorption bands, one in the UV region in the range of 371–418 nm of strong intensity, another in the visible region between 518 and 685 nm, with a weaker intensity, and an even weaker additional band in the near-IR region between 973–1219 nm. The latter band is not observed for $\mathbf{5d}^{\cdot+}$. The high-energy absorptions in the UV appear at similar wavelengths and have comparable intensities to those shown by the corresponding neutral complexes **5a**–**d** and, therefore, they are assigned to localized π-π* transitions at the 2-aza-1,3-butadiene group. The absorptions appearing in the visible region are similar to the bands shown by other oxidized ferrocenyl derivatives and, consequently, are assigned to Cp → Fe^{III} ligand-to-metal charge transfer (LMCT) transitions.[21] Finally, the absorption band in the near-IR, which is not observed in the neutral complexes and is likely to take place after the creation of an electronic vacancy in the HOMO, is assigned to a 2-aza-1,3-butadiene → Fe^{III} LMCT transition. This assignment is based on the following considerations: (i) during the course of the oxidations of **5a**–**c** these low-energy bands increase continuously in intensity, achieving a maximum when the oxidation process is complete (see

 © 2005 Wiley-VCH Verlag GmbH & Co. KGaA, Weinheim

Figure 4); (ii) defined isosbestic points at 385 and 487 nm are maintained during the course of the oxidations (see Figure 4); and (iii) similar low-energy transitions have been observed in the near-IR region in other Fe^{III} and Ru^{III} complexes with conjugated oligothiophene ligands[26,27] and with a -CH_2-N(*R*)-CH_2- bridge.[28] Therefore, the absorption bands in the near-IR shown by **5a**$^{\cdot+}$–**c**$^{+}$ correspond to an optically induced electron transfer from the 2-aza-1,3-butadiene to the Fe^{III} center, as schematically shown in Figure 5 using the Marcus–Hush model.[4] We have assumed that during this optical transition one electron from the localized pair of nonbonding electrons on the N atom of the 2-aza-1,3-butadiene bridge is transferred to the Fe^{III} d_π orbital of the ferrocene moiety. This assumption is supported by the presence of a high-energy filled orbital in oxidized complexes **5a**$^{\cdot+}$–**d**$^{+}$ (e.g. HOMO–2 in **5a**$^{\cdot+}$ and HOMO–3 in **5c**$^{\cdot+}$) that is mainly localized on this N atom, as pointed out by theoretical calculations. Such calculations also show an absolute energetic minimum on the potential energy hypersurface essentially corresponding to the respective neutral top after the appropriate geometrical reorganization to redistribute the electronic density. Only a rough correlation with the experimental absorption values was claimed from time-dependent DFT calculations performed on some of these structures (see Table 4), due to the reported inaccuracy of these types of methods in particular cases.[29] Although there is only a rough correlation between the experimental and calculated values of absorption bands for oxidized complexes **5a**$^{\cdot+}$–**d**$^{\cdot+}$, the results of the time-dependent DFT calculations confirmed the assignations of optical transitions previously given for **5a**$^{\cdot+}$–**d**$^{\cdot+}$, based on experimental facts.

Table 4. Calculated and experimental electronic absorptions of oxidized species **5a**$^{+\cdot}$–**d**$^{+\cdot}$ and **5f**$^{+\cdot}$.

Compound	Calculated λ_{max} [nm] (oscillator strength)		Experimental[a] λ_{max} [nm] (10^{-3} ε, $M^{-1}cm^{-1}$)	
5a$^{+\cdot}$	418.8 (0.1538), 421.1 (0.1415), 486.6 (0.0560), 527.7 (0.0002), 566.0 (0.0014), 618.0 (0.3043)	947.5 (0.0210)	418 (8.5), 481 (3.8), 519 (2.8), 575 (1.9), 618 (0.9)	975 (1.0)
5b$^{+\cdot}$	–	–	259 (16.7), 330 (10.24), 390(sh), 518 (2.29), 685 (0.70)	1219 (0.30)
5c$^{+\cdot}$	269.6 (0.3447), 286.9 (0.1123), 360.0 (0.3045), 414.9 (0.2880), 556.8 (0.2648)	974.5 (0.0275)	259 (9.8), 293 (7.3), 383(7.2), 536 (2.2)	973 (0.13)
5d$^{+\cdot}$	–	–	263 (19.7), 286 (sh), 371(25.2), 549 (4.2)	–
5f$^{+\cdot}$	349.3 (0.1272), 374.2 (0.0753), 425.8 (0.0428), 549.5 (0.0101)	846.0 (0.0027), 1249.4 (0.0017)	327 (12.8), 369 (sh), 429 (sh), 547 (4.9)	764 (0.33), band A; 1250 (0.64) band B
5f^{2+}	–	–	297 (sh), 365 (11.4), 558 (3.7)	764 (0.60), band A; 971 (0.36); band C

[a] In CH_2Cl_2.

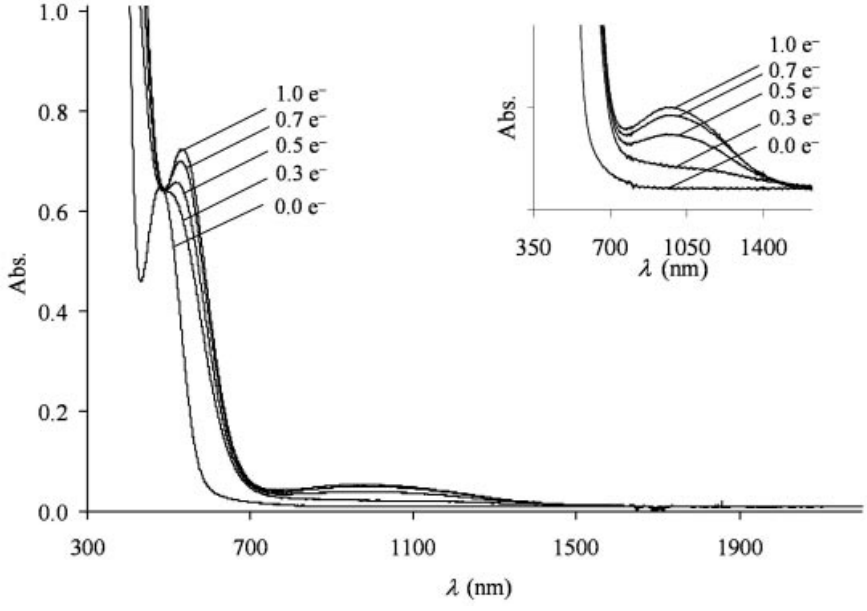

Figure 4. Evolution of Vis-near-IR spectra during the course of the oxidation of compound **5c**. The average number of removed electrons is given on each spectrum. Inset: NIR region enlargement.

 © 2005 Wiley-VCH Verlag GmbH & Co. KGaA, Weinheim

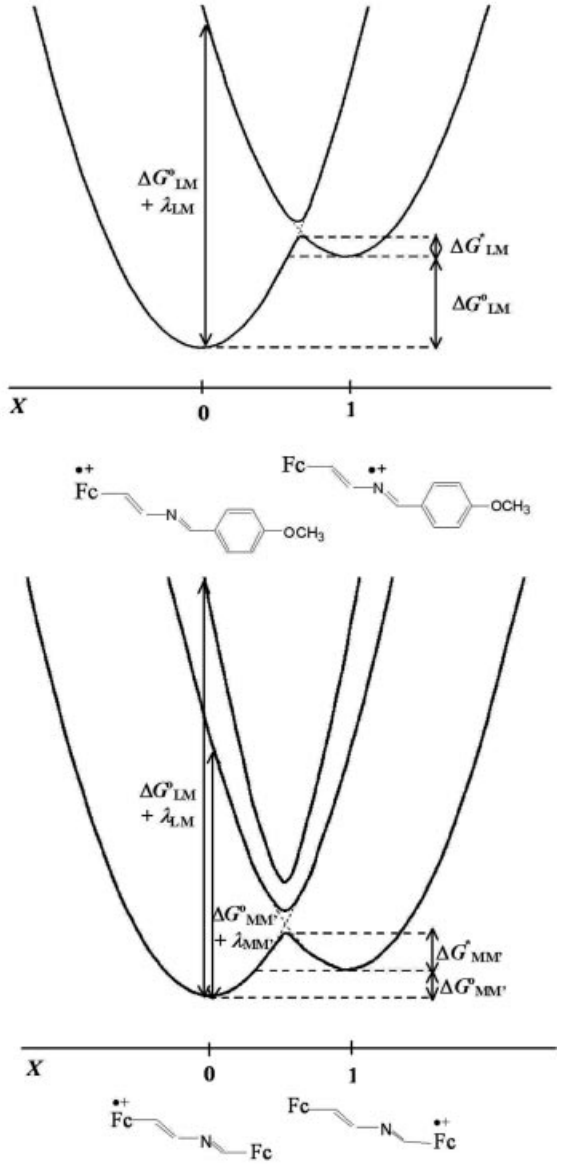

Figure 5. Marcus–Hush model used to describe IET in asymmetric oxidized complexes **5a**$^{\cdot+}$–**d**$^{\cdot+}$ (top) and in oxidized homobimetallic complex **5f**$^{\cdot+}$ (bottom).

The Marcus–Hush model can be used to describe the classical intramolecular electron-transfer process when the electron is coupled between a donor and an acceptor group via a single oscillator having the same frequency in both initial and final states.[4] Originally developed for the interpretation of intervalence charge transfer (IV-CT) bands in extended solids, the Marcus–Hush model has been extended and applied to IV-CT in mixed-valence organometallic[30,31] and organic compounds,[1g,32] as well as to LMCT and metal-to-ligand charge transfer (MLCT) processes in charge-localized asymmetric complexes.[33,34] In accordance with such precedents we have also used the Marcus–Hush model to study the IET of asymmetric complexes **5a**$^{\cdot+}$–**d**$^{\cdot+}$. As schematized in Figure 5, such species exist in two states having the charge/hole localized either on the metal (M) or a particular region of the organic ligand (L), which are separated by the relative free enthalpy $\Delta G°_{LM}$. The electronic coupling between the two electroactive centers (M and L) is measured by the V_{LM} term and the optical transition energy of the LMCT band at its maximum ($h\nu_{max}$; in cm^{-1}), corresponds to the sum of $\Delta G°_{LM}$ and the vertical reorganization energy λ_{LM} (i.e. $h\nu_{max} = \Delta G°_{LM} + \lambda_{LM}$).

The spectral data of LMCT bands of **5a**$^{\cdot+}$–**d**$^{\cdot+}$, summarized in Table 5, can be used to determine the electronic coupling parameter, V_{LM}, and the reorganization energy, λ_{LM}, for each oxidized compound. This was accomplished by deconvoluting the LMCT bands[35] using the classical procedure (see Figure S2 in the Supporting Information) assuming that the effective electron-transfer distance is the distance between the Fe and N atoms. Such distances can be determined from the crystal structures of **5b**, **5d**, and **5f** (5.2 and 3.9 Å for the complexes with the ferrocenyl groups attached to the 4- and 1-positions, respectively). The relative free enthalpies of the two vibronically localized electronic states for compounds **5a**–**c** can be estimated, in a first approximation, from the difference of electrochemical potentials corresponding to the oxidation of the 2-aza-1,3-butadiene center (L) and to the ferrocenyl center (M) of neutral complexes. Due to the experimental impossibility of measuring the L^0/L^{+1} couple of the 2-aza-1,3-butadiene when it is linked to a neutral ferrocenyl group, the corresponding oxidation potential was assumed to be 40 mV less positive than the anionic peak of compound **5e**, observed at +1.084 V, since the *p*-methoxyphenyl and ferrocenyl groups have similar electron-donor capabilities but the first group is not electrochemically active at potentials lower than +1.4 V (vide supra). An inspection of the resulting V_{LM} val-

Table 5. LMCT and IV-CT band parameters, obtained from the spectral deconvolution, and calculated IET parameters for radical cations **5a**$^{+\cdot}$–**d**$^{+\cdot}$and **5f**$^{+\cdot}$.

	R^1	R^2	ΔG^0_{LM} [cm^{-1}]	$h\nu_{max}$ [cm^{-1}]	λ_{LM} [cm^{-1}]	ε_{max} [M^{-1} cm^{-1}]	$\Delta\nu_{1/2}$ [cm^{-1}]	f[a]·10^3	d [Å]	V_{LM} [cm^{-1}]
5a$^{+\cdot}$	4-$CH_3OC_6H_4$	Fc	4150	10260	6110	1000	2640	12.1	5.2	650
5b$^{+\cdot}$	4-$NO_2C_6H_4$	Fc	3660	8200	4540	300	2090	2.9	5.2	280
5c$^{+\cdot}$	Fc	4-$CH_3OC_6H_4$	2790	10280	7490	130	3800	2.3	3.9	380
5d$^{+\cdot}$	Fc	4-$NO_2C_6H_4$	2740	–	–	–	–	–	–	–
5f$^{+\cdot}$	Fc	Fc	3900	13090[b] (band A)	9190[b]	330[b]	3450[b]	5.2[b]	5.2	480[b]
			1110	8000[c] (band B)	6890[c]	640[c]	2500[c]	7.4[c]	9.1	260[c]

[a] Total oscillator strength obtained by $f = 4.6\times10^{-9}\ \varepsilon_{max}\cdot\Delta\nu_{1/2}$. [b] LMCT band corresponding to an electron transfer between L and M units. [c] IV-CT band corresponding to an electron transfer between M and M′ units.

 © 2005 Wiley-VCH Verlag GmbH & Co. KGaA, Weinheim

ues for complexes **5a**–**c** (Table 5) shows that electronic couplings between the ferrocenyl and the 2-aza-1,3-butadiene ligand are moderate, such that all these complexes belong to class II.[8] In addition, the electronic coupling of complexes **5a**–**c** is influenced by the position to which the ferrocenyl is attached, as well as on the electron-donor capability of the substituent on the phenyl group. It should be noted from the spectral analysis that the charge-transfer transition oscillator strengths clearly increase for complexes **5a**–**d**. Complex **5d** apparently does not show any LMCT band. This can be ascribed to the presence of a nitro group linked to the 4-position of the bridge, which drains some electron density from the 2-aza-1,3-butadiene chain, thus lowering the effective overlap between diabatic orbitals and decreasing the probability of the transition. This effect has indeed been predicted theoretically for other electron-withdrawing groups, such as the cyano group.[36]

Intramolecular Electron Transfer in the Mixed-Valence Compound $5f^{+\cdot}$

Oxidized species derived from **5f** were generated electrochemically and their formation followed by absorption spectroscopy. Thus, a stepwise coulometric titration was performed on a 2×10^{-3} M solution of **5f** in CH_2Cl_2, with $[(n\text{Bu})_4\text{N}]PF_6$ (0.15 M) as supporting electrolyte, and absorption spectra were regularly recorded for a different average number ($0 \le n \le 2$) of removed electrons. Figure 6a shows the evolution of the spectra during the oxidation of **5f** in the $0 \le n \le 1$ range, with an increase of the Cp → Fe^{III} LMCT band appearing at 547 nm, characteristic of a ferrocenium ion, and a decrease of the band that corresponds to a localized excitation of a ferrocene group at 478 nm. Along with the changes of these bands, the appearance and maintenance of two well-defined isosbestic points at 425 and 501 nm was observed. Nevertheless, the most interesting feature is that during the oxidation of **5f** two new weak and broad bands centered at 764 nm (band A) and at 1250 nm (band B) appear, and these increase continuously in intensity until one electron has been removed (i.e. when the formation of $\mathbf{5f}^{+\cdot}$ is complete). As also shown in Figure 6, on removing more electrons ($1 \le n \le 2$) the intensity of band A continues to increase until its intensity has doubled, while band B decreases until it disappears (when the dication $\mathbf{5f}^{2+}$ is completely formed). At the same time, another new weak and broad band at 971 nm (band C) increases until the fully oxidized species $\mathbf{5f}^{2+}$ is formed. Table 4 collects all the spectroscopic data for oxidized complexes $\mathbf{5f}^{+\cdot}$ and $\mathbf{5f}^{2+}$. The deconvolution of the experimental spectra of $\mathbf{5f}^{+\cdot}$, performed on spectral intensity times wavenumber vs. wavenumber, assuming Gaussian shapes (Figure 6c), allows an accurate determination of the position, width, and intensity of bands A and B, which are gathered in Table 5.[35,37] These spectral parameters are relevant for the characterization of intramolecular electron transfer in $\mathbf{5f}^{+\cdot}$

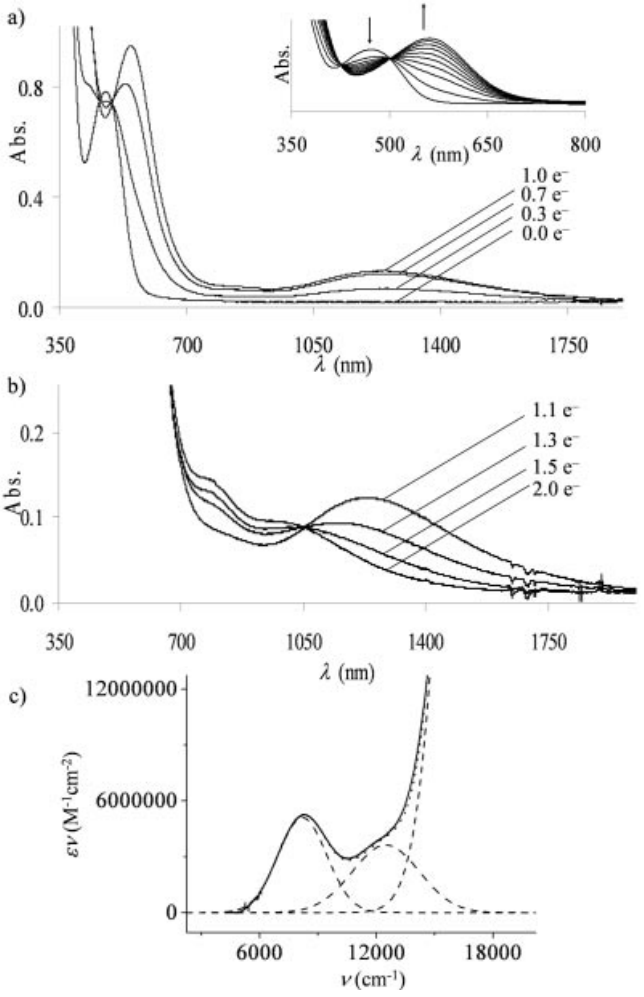

Figure 6. Evolution of Vis-near-IR spectra upon oxidation of **5f**: a) oxidation of **5f** until the maximum ($n = 1$) of the mixed-valence species $\mathbf{5f}^{+\cdot}$ is achieved. Inset: Expanded spectra of the visible region showing the two isosbestic points; b) oxidation until the maximum ($n = 2$) of the fully oxidized species $\mathbf{5f}^{2+}$ is achieved; c) deconvolution of the NIR spectrum of the $\mathbf{5f}^{+\cdot}PF_6^{-\cdot}$ salt. The experimental spectrum was deconvoluted by means of three Gaussian functions (dashed lines) using spectral intensity times wavenumber vs. wavenumber. The sum of the dashed lines (dotted line) closely matches the experimental spectrum (solid line).

The presence of several near-IR bands in the spectrum of a mixed-valence complex is not uncommon, and their occurrence is generally explained by one of three different possible causes.[38,39] One could be the presence of a strong spin-orbit coupling effect, which becomes important only for complexes containing third-row transition metals.[38] A second source could be the presence of a double-exchange mechanism,[39] a mechanism that becomes more probable as the bridge length and the level of π-orbitals increases. Finally, such multiple near-IR bands might be caused by the presence of a bridge with accessible redox state levels, as has been recently proposed to explain the rich absorption spectrum of certain mixed-valence compounds with redox-active bridges.[1g] Based on the behaviors of $\mathbf{5a}^{+\cdot}$–$\mathbf{c}^{+\cdot}$, the latter source seems to be the most probable origin for the

 © 2005 Wiley-VCH Verlag GmbH & Co. KGaA, Weinheim

two near-IR bands of **5f**$^{+\cdot}$. Accordingly, and also based on the spectral evolution observed during the oxidation of **5f**, the band A is assigned to a 2-aza-1,3-butadiene → Fe^{III} LMCT transition, which implies an electron transfer from the N atom of the 2-aza-1,3-butadiene bridge to the Fe^{III} site linked at the 4-position of the bridge, whereas band B is attributed to the bridge-mediated superexchange between the two coupled iron sites (M and M′) − an IET between the two iron sites.

In order to estimate the effectiveness of both IET pathways we used the Marcus–Hush model, as schematized in Figure 5, where the reorganization energies of both transitions, λ_{LM} and $\lambda_{MM'}$, were determined from the absorption maxima of the bands A and B. For the free-energy difference between the two electronic states of **5f**$^{+\cdot}$ having the charge localized on each Fe site we used, in a first approximation, the value of $\Delta G°_{MM'}$ (1113 cm^{-1}) obtained from the difference of the first oxidation potentials of **5c** and **5f**. For $\Delta G°_{LM}$ we used a value of 3904 cm^{-1}, which was determined by employing the same approximations as for **5a**$^{+\cdot}$–**c**$^{+\cdot}$ (vide supra). The spectral parameters of bands A and B were also used to determine the effective electronic coupling parameters V_{LM} and $V_{MM'}$, taking as effective electron-transfer distances those measured between the N and the two Fe atoms in the crystal structure of **5f**. Both effective electronic couplings are moderate, indicating that the mixed-valence **5f**$^{+\cdot}$ also belongs to class II.[8] The relative values of V_{LM} and $V_{MM'}$ indicate that the IET may proceed through the two different pathways. The IET mediated by the bridge through a superexchange is apparently less effective than that in which the electron jumps into the bridge. It is also of interest to compare the effective electronic coupling between the two iron sites of **5f**$^{+\cdot}$ with that of the mixed-valence compound derived from 1,4-diferrocenyl-1,3-butadiene, i.e., $[Fc(CH=CH)_2Fc]^{+\cdot}$.[14] The latter compound has a $V_{MM'}$ of 430 cm^{-1}, which is larger than that of **5f**$^{+\cdot}$, suggesting that the replacement of an sp^2 C atom by an N atom in the 1,3-butadiene bridge results in a decrease of the interaction between both ferrocenes, probably because of a poorer overlap between the diabatic orbitals of the two ferrocenes with the orbital of the bridge involved in the superexchange mechanism. Indeed, in both types of systems the HOMO of the neutral molecule is the bridge-centered superexchange involved MO, which can be considered as being formed by a combination of the higher energy MO of π-type at the bridge and two $3e_2'$-based MOs of both ferrocene subunits (Figure 7). At the level of theory used, the latter is 0.953 eV higher in energy than the HOMO in 1,3-butadiene, but 1.587 eV higher than HOMO–1 in the 2-aza-1,3-butadiene, the HOMO being that containing the electron lone-pair at the N atom. (See Figure S3 in the Supporting Information). This leads to a poorer, although still significant, overlap between the diabatic orbitals of the two ferrocenes with the orbital of the bridge involved in the superexchange mechanism.

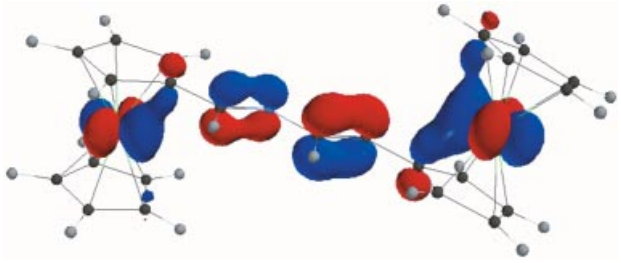

Figure 7. Superexchange-responsible MO (HOMO) in compound **5f** at a 0.050 isovalue.

For the mixed-valence **5f**$^{+\cdot}$ the free energy difference between the two electronic states having the charge localized on each Fe site is 3.2 kcal mol^{-1}. This relatively large value suggests that, at 300 K, the population of the state with the positive charge located on the iron attached to the 4-position of the 2-aza-1,3-butadiene bridge is dominant, with just a very small population (<0.1%) of the state with the charge on the other iron site. In addition, we can make a crude estimation of the thermal activation energy barrier for the interconversion of such two states, using the Marcus–Hush model.[40,41] The resulting thermal energy barrier of about 7.4 kcal mol^{-1} suggests a rate constant of about 10^8 s^{-1} at 300 K and hence any spectroscopic technique with a time scale faster than 10^9 s^{-1} should show the valence-localized mixed-valence complex **5f**$^{+\cdot}$, with the positive charge trapped on the Fe site attached at the 4-position of the bridge, at this temperature. This effect would be even more pronounced at temperatures below 100 K, so that with spectroscopic techniques such ^{57}Fe Mössbauer and EPR the valence should appear to be localized, as is indeed the case (see Supporting Information).

Conclusion and Perspectives

The presence of low-energy LMCT and IV-CT bands in the oxidized forms **5a**$^{+\cdot}$–**d**$^{+\cdot}$ and **5f**$^{+\cdot}$ of mono- and bis-ferrocenyl derivatives attached to a 2-aza-1,3-butadiene bridge indicates the existence of optically induced IETs between the metal units and the organic linkers. This important result demonstrates that the introduction of a heteroatom, like the N atom, in a conjugated organic bridge is an attractive strategy for promoting IET through an alternative pathway. This finding may have implications in the design of molecular electron-transfer materials and, in particular, in the development of new molecular devices that act as electronic relays which promote IET over large distances. Efforts in this direction are in progress in our laboratories using symmetrical compounds with two electroactive units attached to oxidizable, symmetrical, and conjugated organic bridges containing two heteroatoms.

Experimental Section

General Procedures: All reactions were carried out under N_2 and using solvents which were dried by routine procedures. All melting points were determined on a Kofler hot-plate melting point apparatus and are uncorrected. IR spectra were determined as Nujol emulsions or films on a Nicolet Impact 400 spectrophotometer. UV/Vis–near IR spectra were recorded on a Varian Cary 5 E spec-

 © 2005 Wiley-VCH Verlag GmbH & Co. KGaA, Weinheim

trophotometer. ^{1}H and ^{13}C NMR spectra were recorded on a Bruker AC200, 300, or 400 spectrometer (200, 300, or 400 MHz for ^{1}H). Chemical shifts are referenced to signals of tetramethylsilane in the case of ^{1}H and ^{13}C NMR spectra and to 85% aqueous phosphoric acid in the case of ^{31}P NMR spectra. The EI and FAB$^+$ mass spectra were recorded on a Fisons AUTOSPEC 500 VG spectrometer, using 3-nitrobenzylalcohol as matrix. EPR spectra were obtained with an X-Band Bruker ESP 300E spectrometer equipped with a TE_{102} microwave cavity, a Bruker variable temperature unit, a field frequency lock system Bruker ER 033 M; line positions were determined with an NMR Gaussmeter Bruker ER 035 M. The modulation amplitude was kept well below the line width, and the microwave power was well below saturation. Crystallographic measurements were made at 233(2) K on a Bruker diffractometer equipped with an area detector positioned at the window of a rotating anode generator using Mo-K_α radiation (λ = 0.71073 Å). Mössbauer spectra were recorded on an ES-Technology MS-105 spectrometer, with a 100 MBq ^{57}Co source, in a rhodium matrix. Solid samples were prepared by grinding with boron nitride. Spectra were referenced to natural iron at 298 K. Parameters were obtained by fitting the data with Lorentzian lines; errors <0.01 mm s^{-1}. Microanalyses were performed on a Perkin–Elmer 240C instrument. The cyclic voltammetric measurements were performed on a QUICELTRON potentiostat/galvanostat controlled by a personal computer and driven by dedicated software. Cyclic voltammetry was performed with a conventional three-electrode configuration consisting of platinum working and auxiliary electrodes and an SCE reference electrode. The experiments were carried out with a 10^{-3} M solution of sample in dry CH_2Cl_2 containing 0.1 M $[N(nC_4H_9)_4]ClO_4$ as supporting electrolyte. Deoxygenation of the solutions was achieved by bubbling nitrogen for at least 10 min and the working electrode was cleaned after each run. The cyclic voltammograms were recorded with a scan rate increasing from 0.05 to 1.00 V s^{-1}. The square-wave voltammograms were recorded before and after addition of sequential additions of an aliquot of 0.1 equiv. of 2.5×10^{-2} M solutions of $HBF_4 \cdot Et_2O$ in CH_3CN. ΔE_s = 4 mV, ΔE_p = 25 mV, and f = 15 Hz. Decamethylferrocene (DMFe) (–0.07 V vs. SCE) was used as an internal reference both for potential calibration and for reversibility criteria. Oxidations were performed by electrolysis in a three-electrode cell under argon using dry CH_2Cl_2 as solvent and 0.15 M $[N(n\text{-}C_4H_9)_4]ClO_4$ as supporting electrolyte. The progress of the oxidation was followed coulometrically (or chronoamperometrically) by 263A of EG&PAR potentiostat-galvanostat. The reference electrode and the counter electrode were separately immersed in the solvent containing the supporting electrolyte and isolated from the bulk solution by a glass frit. The working electrode was a platinum grid. UV/Vis–near IR absorption spectra were regularly recorded by transferring a small aliquot of the solution contained in the electrochemical cell into a UV quartz cell for a different average number of removed electrons.

Theoretical Calculations: Geometry optimizations were performed with the Spartan'02 package (Spartan'02, build 119, Wavefunction Inc., Irvine, CA). For neutral compounds **5a**–**f** a preliminary optimization was done at the semi-empirical PM3(d) level and the obtained geometries were then refined at the DFT level of theory,[42] which has proved to be remarkably successful in reproducing experimental ground-state geometries and rotational barriers for ferrocenes.[43] The B3LYP functional[44] (Becke's three-parameter hybrid functional[45] with the Lee–Yang–Parr[46] correlation functional) and the 3-21G* basis set were used. Harmonic frequency calculations verified the nature of the stationary points as minima (all real frequencies).[47] The geometry of oxidized radical-cation species **5a**$^{+\cdot}$, **5c**$^{+\cdot}$, **5d**$^{+\cdot}$, and **5f**$^{+\cdot}$ were optimized starting from the corresponding neutral minimized structures with the appropriate charge and multiplicity constraints. Structure **5b**$^{+\cdot}$ was not calculated due to systematic failures in the SCF convergence. Similarly, **5f**$^{+\cdot}$ was used as the initial geometry for the fully oxidized **5f**$^{2+}$. Time-dependent DFT methods (TDDFT), as contained within the Gaussian 98 program suite,[48] performed as an SPE calculation at the same level as the minimized structures, were employed to study the excited states and model the UV/Vis–NIR electronic transitions in both neutral and oxidized species.

General Procedure for the Preparation of Diethyl *N*-Arylidene- and [(Ferrocenylmethylidene)aminomethyl]phosphonates 3: A mixture of diethyl aminomethylphosphonate (0.78 g, 4.64 mmol), an equimolar amount of the appropriate aldehyde **2**, and *p*-toluenesulfonic acid (0.01 g, 0.058 mmol) in dry benzene (50 mL) was stirred at room temperature for 4 h. Then, the flask was fitted with a Dean–Stark trap and a reflux condenser and heated overnight, atr reflux temperature, with constant removal of water. The reaction mixture was allowed to cool to room temperature and the solvent was removed under vacuum to give the corresponding diethyl phosphonates **3** as colored oils, which were used without further purification in the next step.

Diethyl [(*p*-Methoxybenzylidene)aminomethyl]phosphonate (3a): Yield: 95%. IR (Nujol): $\tilde{\nu}$ = 1641, 1609, 1577, 1524, 1444, 1422, 1396, 1316, 1252, 1166, 1102, 969 cm^{-1}. ^{1}H NMR ($CDCl_3$): δ = 1.34 (t, $^4J_{H,P}$ = 6.5 Hz, 6 H), 3.84 (s, 3 H), 4.07 (d, $^1J_{H,P}$ = 16.8 Hz, 2 H),4.19–4.09 (m, 4 H), 6.91 (d, J = 8.6 Hz, 2 H), 7.68 (d, J = 8.6 Hz, 2 H), 8.22 (d, $^4J_{H,P}$ = 4.7 Hz, 1 H) ppm. ^{13}C NMR ($CDCl_3$): δ = 16.5 (d, $^3J_{P,C}$ = 5.6 Hz, CH_3), 55.3 (CH_3O), 57.4 (d, $^1J_{P,C}$ = 152.6 Hz, NCH_2), 62.4 (d, $^2J_{P,C}$ = 6.7 Hz, OCH_2), 114.0 (CH_{Ar}), 128.7 (q), 130.0 (CH_{Ar}), 162.0 (q), 164.9 (d, $^3J_{P,C}$ = 16.0 Hz, CH=N) ppm. ^{31}P NMR ($CDCl_3$): δ = 22.68 ppm. EIMS: m/z (%) = 285 (100) [M$^+$], 152 (82), 148 (61), 125 (90), 121 (80), 97 (44), 91 (19), 78 (25).

Diethyl [(*p*-Nitrobenzylidene)aminomethyl]phosphonate (3b): Yield: 85%. IR (Nujol): $\tilde{\nu}$ = 1654, 1604, 1523, 1454, 1404, 1360, 1266, 1097, 1016, 966, 847 cm^{-1}. ^{1}H NMR ($CDCl_3$): δ = 1.34 (t, $^4J_{H,P}$ = 6.9 Hz, 6 H), 4.01–4.24 (m, 6 H), 7.91 (d, J = 8.0 Hz, 2 H), 8.26 (d, J = 8.0 Hz, 2 H), 8.40 (d, $^4J_{H,P}$ = 5.1 Hz, 1 H) ppm. ^{13}C NMR ($CDCl_3$): δ = 16.4 (d, $^3J_{P,C}$ = 5.7 Hz, CH_3), 57.7 (d, $^1J_{P,C}$ = 152.7 Hz, NCH_2), 62.7 (d, $^2J_{P,C}$ = 6.6 Hz, OCH_2), 123.8 (CH_{Ar}), 130.5 (CH_{Ar}), 140.9 (q), 149.2 (q), 163.2 (d, $^3J_{P,C}$ = 22.0 Hz, CH=N) ppm. ^{31}P NMR ($CDCl_3$): δ = 21.77 ppm. EIMS: m/z (%) = 300 (36) [M$^+$], 163 (60), 152 (96), 125 (82), 108 (100), 90 (95), 81 (42).

Diethyl [(Ferrocenylmethylidene)aminomethyl]phosphonate (3c): Yield: 94%. IR (Nujol): $\tilde{\nu}$ = 1642, 1473, 1448, 1398, 1241, 1166, 1035, 972, 828, 778 cm^{-1}. ^{1}H NMR ($CDCl_3$): δ = 1.38 (t, $^4J_{H,P}$ = 3.3 Hz, 6 H), 3.92 (d, 2 H, $^2J_{H,P}$ = 18 Hz), 4.08–4.25 (m, 4 H), 4.23 (s, 5 H), 4.36 (t, J = 1.8 Hz, 2 H), 4.64 (t, J = 1.8 Hz, 2 H), 8.19 (d, $^4J_{H,P}$ = 4.8 Hz, 1 H) ppm. ^{13}C NMR ($CDCl_3$): δ = 16.3 (d, $^3J_{P,C}$ = 5.7 Hz, CH_3), 57.2 (d, $^1J_{P,C}$ = 150.7 Hz, NCH_2), 62.4 (d, $^2J_{P,C}$ = 6.5 Hz, OCH_2), 68.5 (2 × CH, Cp), 69.1 (5 × CH, Cp), 70.6 (2 × CH, Cp), 79.7 (d, $^4J_{P,C}$ = 9 Hz, q, Cp), 166.2 (d, $^3J_{P,C}$ = 19.5 Hz, CH=N) ppm. ^{31}P NMR ($CDCl_3$): δ = 22.77 ppm. EIMS: m/z (%) = 363 (86) [M$^+$], 298 (100), 224 (39), 260 (48), 121 (63), 81 (25), 65 (9), 56 (24).

General Procedure for the Preparation of 1,4-Disubstituted-2-aza-1,3-butadienes 5: *n*-Butyllithium (1.6 M in hexane, 3 mL) was added dropwise to a solution of the appropriate diethyl phosphonate **3** (4.64 mmol) in dry THF (20 mL) at –78 °C under nitrogen. A solution of an equimolar amount of the appropriate aldehyde **4** (4.64 mmol) in dry THF (10 mL) was added dropwise to this stirred

 © 2005 Wiley-VCH Verlag GmbH & Co. KGaA, Weinheim

solution and the mixture was stirred for 1.5 h. Then, the reaction mixture was allowed to reach room temperature and was heated at reflux temperature overnight. After the solution had cooled to room temperature, the solvent was evaporated under reduced pressure and the crude product was stirred with water (50 mL) and then extracted with dichloromethane (4 × 50 mL). The combined organic layers were dried with anhydrous Na_2SO_4 and, after filtration, the solution was concentrated to dryness to give a crude product which was crystallized from dichloromethane/diethyl ether (1:10).

4-Ferrocenyl-1-(*p*-methoxyphenyl)-2-aza-1,3-butadiene (5a): Yield: 90%; m.p. 175–176 °C. IR (Nujol): $\tilde{\nu}$ = 1605, 1511, 1456, 1395, 1240, 1162, 1107, 1074, 1046, 1024, 990, 985, 830, 741 cm^{-1}. ^1H NMR ($CDCl_3$): δ = 3.86 (s, 3 H), 4.15 (s, 5 H), 4.28 (t, J = 1.6 Hz, 2 H), 4.43 (t, J = 1.6 Hz, 2 H), 6.70 (d, J = 14.0 Hz, 1 H), 6.94 (d, J = 8.0 Hz, 2 H), 7.18 (d, J = 14.0 Hz, 1 H), 7.75 (d, J = 8.0 Hz, 2 H), 8.18 (s, 1 H) ppm. ^{13}C NMR ($CDCl_3$): δ = 55.3 (CH_3O), 67.0 (2 × CH, Cp), 69.0 (2 × CH, Cp), 69.3 (5 × CH, Cp), 81.5 (q, Cp), 114.2 (CH_{Ar}), 128.3 (CH=CH), 129.4 (q), 129.9 (CH_{Ar}), 139.7 (CH=CH), 158.0 (q), 161.5 (CH=N) ppm. EIMS: m/z (%) = 345 (100) [M^+], 280 (77), 278 (10), 121 (31), 56 (23). $C_{20}H_{19}FeNO$ (345.22): calcd. C 69.58, H 5.55, N 4.06; found C 69.35, H 5.40, N 4.15.

4-Ferrocenyl-1-(*p*-nitrophenyl)-2-aza-1,3-butadiene (5b): Yield: 50%; m.p. 223–224 °C. IR (Nujol): $\tilde{\nu}$ = 1600, 1514, 1454, 1335, 1182, 1109, 1030, 957, 745, 698 cm^{-1}. ^1H NMR ($CDCl_3$): δ = 4.12 (s, 5 H), 4.32 (t, J = 1.6 Hz, 2 H), 4.42 (t, J = 1.6 Hz, 2 H), 6.87 (d, J = 13.0 Hz, 1 H), 7.21 (d, J = 13.0 Hz, 1 H), 7.89 (d, J = 8.1 Hz, 1 H), 8.22 (s, 1 H), 8.23 (d, J = 8.1 Hz, 1 H) ppm. ^{13}C NMR ($CDCl_3$): δ = 67.5 (2 × CH, Cp), 69.6 (5 × CH, Cp), 69.9 (2 × CH, Cp), 80.4 (q), 124.2 (CH_{Ar}), 128.5 (CH_{Ar}), 134.0 (CH=CH), 138.6 (CH=CH), 142.3 (q), 148.5 (q), 154.7 (CH=N) ppm. EIMS: m/z (%) = 360 (100) [M^+], 330 (19), 295 (23), 265 (21), 192 (34), 165 (30), 121 (62). $C_{19}H_{16}FeN_2O_2$ (360.19): calcd. C 63.36, H 4.48, N 7.78; found C 63.54, H 4.35, N 7.69.

1-Ferrocenyl-4-(*p*-methoxyphenyl)-2-aza-1,3-butadiene (5c): Yield: 85%; m.p. 102–103 °C. IR (Nujol): $\tilde{\nu}$ = 1645, 1605, 1565, 1514, 1250, 1176, 1107, 1038, 969, 826 cm^{-1}. ^1H NMR ($CDCl_3$): δ = 3.82 (s, 3 H), 4.22 (s, 5 H), 4.47 (t, J = 1.6 Hz, 2 H), 4.73 (t, J = 1.6 Hz, 2 H), 7.34 (d, J = 14.0 Hz, 1 H), 7.40 (d, J = 8.0 Hz, 2 H), 7.82 (d, J = 14.0 Hz, 1 H), 7.88 (d, J = 8.0 Hz, 2 H), 8.21 (s, 1 H) ppm. ^{13}C NMR ($CDCl_3$): δ = 55.2 (CH_3O), 68.7 (2 × CH, Cp), 68.9 (5 × CH, Cp), 71.1 (2 × CH, Cp), 80.4 (q), 114.1 (CH_{Ar}), 127.5 (CH_{Ar}), 127.6 (CH=CH), 129.3 (q), 141.0 (CH=CH), 159.0 (q), 161.5 (CH=N) ppm. EIMS: m/z (%) = 345 (100) [M^+], 318 (40), 279 (24), 278 (14), 186 (43), 121 (66), 56 (39). $C_{20}H_{19}FeNO$ (345.22): calcd. C 69.58, H 5.55, N 4.06; found C 69.33, H 5.28, N 4.21.

1-Ferrocenyl-4-(*p*-nitrophenyl)-2-aza-1,3-butadiene (5d): Yield: 40%; m.p. 182–183 °C. IR (Nujol): $\tilde{\nu}$ = 1561, 1508, 1438, 1337, 1225, 1177, 1123, 1107, 1033, 750, 696 cm^{-1}. ^1H NMR ($CDCl_3$): δ = 4.24 (s, 5 H), 4.56 (t, J = 1.6 Hz, 2 H), 4.78 (t, J = 1.6 Hz, 2 H), 6.87 (d, J = 13.4 Hz, 1 H), 7.52 (d, J = 8.0 Hz, 2 H), 7.55 (d, J = 13.4 Hz, 1 H), 8.18 (d, J = 8.0 Hz, 2 H), 8.35 (s, 1 H) ppm. ^{13}C NMR ($CDCl_3$): δ = 69.4 (2 × CH, Cp), 69.6 (5 × CH, Cp), 72.1 (2 × CH, Cp), 79.6 (q), 124.2 (CH_{Ar}), 125.2 (CH=CH), 126.6 (CH_{Ar}), 143.7 (q), 146.4 (q), 146.5 (CH=CH), 165.9 (CH=N) ppm. EIMS: m/z (%) = 360 (100) [M^+], 333 (22), 192 (22), 186 (34), 165 (27), 120 (63), 56 (33). $C_{19}H_{16}FeN_2O_2$ (360.19): calcd. C 63.36, H 4.48, N 7.78; found C 63.19, H 4.29, N 7.62.

1,4-Bis(*p*-methoxyphenyl)-2-aza-1,3-butadiene (5e): Yield: 85%; m.p. 170–172 °C. IR (Nujol): $\tilde{\nu}$ = 1647, 1609, 1553, 1510, 1454, 1423, 1373, 1311, 1280, 1255, 1174, 1111, 1024, 986, 943, 875, 813 cm^{-1}. ^1H NMR ($CDCl_3$): δ = 3.80 (s, 3 H), 3.84 (s, 3 H), 6.86 (d, J = 8.0 Hz, 2 H), 6.91 (d, J = 14.1 Hz, 1 H), 6.94 (d, J = 8.0 Hz, 2 H), 7.40 (d, J = 8.0 Hz, 2 H), 7.44 (d, J = 14.1 Hz, 1 H), 7.76 (d, J = 8.0 Hz, 2 H), 8.25 (s, 1 H) ppm. ^{13}C NMR ($CDCl_3$): δ = 55.2, 55.3, 114.0, 114.1, 127.8, 129.2, 129.4, 130.0, 140.4, 159.2, 159.7, 161.8 ppm. EIMS: m/z (%) = 267 (100) [M^+], 252 (44), 236 (28), 160 (69), 121 (35), 91 (28). $C_{17}H_{17}NO_2$ (267.33): calcd. C 76.38, H 6.41, N 5.24; found C 76.20, H 6.67, N 5.12.

1,4-Bis(ferrocenyl)-2-aza-1,3-butadiene (5f): Yield: 87%; m.p. 253–255 °C. IR (Nujol): $\tilde{\nu}$ = 1649, 1580, 1102, 1023, 1041, 1003, 966, 829, 810 cm^{-1}. ^1H NMR ($CDCl_3$): δ = 4.15 (s, 5 H), 4.22 (s, 5 H), 4.27 (s, 2 H), 4.40 (s, 2 H), 4.45 (s, 2 H), 4.72 (s, 2 H), 6.60 (d, J = 13.2 Hz, 1 H), 7.05 (d, J = 13.2 Hz, 1 H), 8.11 (s, 1 H) ppm. ^{13}C NMR ($CDCl_3$): δ = 66.80 (2 × CH, Cp), 68.61 (2 × CH, Cp), 69.00 (2 × CH, Cp), 69.20 (10 × CH, Cp), 71.00 (2 × CH, Cp), 80.81 (q, Cp), 82.11 (q, Cp), 126.32 (CH=), 140.32 (=CH-N), 159.82 (CH=N) ppm. EIMS: m/z (%) = 423 (100) [M^+], 358 (60), 212 (32), 186 (28), 121 (64), 56 (25). $C_{23}H_{21}Fe_2N$ (423.12): calcd. C 65.29, H 5.00, N 3.31; found C 65.40, H 4.88, N 3.50.

Preparation of the Mixed-Valence Compound $5f^+I_3^-$: A sample of this mixed-valence compound was prepared by adding a solution of iodine (0.030 g, 0.12 mmol) in dry benzene (5 mL) to a solution of 1,4-diferrocenyl-2-aza-1,3-butadiene (0.1 g, 0.24 mmol) in the same solvent (50 mL). The reaction mixture was stirred at room temperature under nitrogen for 1 h and the dark-purple microcrystals formed were collected by filtration and washed with three portions of benzene and one portion of diethyl ether. The solid obtained was dried in a dessicator overnight. FAB MS: m/z (%) = 424 (100) [M^+ + 1]. $C_{23}H_{21}Fe_2I_3N$ (803.82): calcd. C 34.33, H 2.61, N 1.74; found C 34.23, H 2.38, N 1.58.

Supporting Information: Crystal data of **5b**, **5d**, and **5f**, optical absorption data of oxidized species and the procedure for their analysis with the Marcus–Hush model, and ^{57}Fe Mössbauer and EPR spectra are provided.

Acknowledgments

We gratefully acknowledge the financial support of the DGI, Ministerio de Ciencia y Tecnología, Spain (projects MAT2003-04699 and CTQ2004-02201), the Fundación Séneca (CARM) (project no. PB/72/FS/02), and DGR, Catalunya (2001 SGR00362). The Biotechnology and Biological Sciences Research Council, UK, is also thanked for funding (D.J.E.).

[1] a) D. Segal, A. Nitzan, W. B. Davis, M. R. Wasielewski, M. A. Ratner, *J. Phys. Chem. B.* **2000**, *104*, 3817–3829; b) M. N. Paddow-Row, in *Electron Transfer in Chemistry* (Ed.: V. Balzani), Wiley-VCH, Weinheim, **2001**, pp. 179–271; c) L. DeCola, P. Belser, in *Electron Transfer in Chemistry* (Ed.: V. Balzani), Wiley-VCH, Weinheim, **2001**, pp. 97–136; d) K. Kilsa, J. Kajanus, A. N. Macpherson, J. Martensson, B. Albinsson, *J. Am. Chem. Soc.* **2001**, *123*, 3069–3080; e) J.-P. Launay, *Chem. Soc. Rev.* **2001**, *30*, 386–397; f) M. D. Newton, *Chem. Rev.* **1991**, *91*, 767–792; g) S. F. Nelsen, R. F. Ismagilov, D. F. Powell, *J. Am. Chem. Soc.* **1998**, *120*, 1924–1925; h) W. B. Davis, W. A. Svec, M. A. Ratner, M. R. Wasielewski, *Nature* **1998**, *396*, 60–53; i) D. S. Weiss, J. R. Cowdery, R. H. Young, in *Electron Transfer in Chemistry* (Ed.: V. Balzani), Wiley-VCH, Weinheim, **2001**, pp. 379–471; j) H. Bassler, in *Semiconducting Polymers* (Eds.: G. Hadziioannou, P. F. van Hutten), Wiley-VCH, Weinheim, **2000**, pp. 365–410.

 © 2005 Wiley-VCH Verlag GmbH & Co. KGaA, Weinheim

[2] a) U. T. Müller-Westerhoff, *Angew. Chem. Int. Ed. Engl.* **1986**, *25*, 702–717; b) E. E. Bunel, P. Campos, J. Ruz, L. Valle, I. Chadwick, M. Santa Ana, G. Gonzalez, J. M. Manriquez, *Organometallics* **1988**, *7*, 474–476; c) E. E. Bunel, L. Valle, N. L. Jones, P. J. Carroll, M. Gonzalez, N. Muñoz, J. M. Manriquez, *Organometallics* **1988**, *7*, 789–791; d) H. Atzkern, B. Huber, F. H. Köhler, G. Müller, R. Müller, *Organometallics* **1991**, *10*, 238–244; e) J. Hiermeier, F. H. Köhler, G. Müller, *Organometallics* **1991**, *10*, 1787–1793.

[3] a) A. C. Benniston, V. Goulle, A. Harriman, J. M. Lehn, B. Marczinke, *J. Phys. Chem.* **1994**, *98*, 7798–7804; b) M. Haga, M. M. Ali, S. Koseki, K. Fujimoto, A. Yoshimura, K. Nozaki, T. Ohno, K. Nakajima, D. J. Stufkens, *Inorg. Chem.* **1996**, *35*, 3335–3347; c) M. E. Elliot, D. L. Derr, S. Ferrere, M. D. Newton, Y. P. Liu, *J. Am. Chem. Soc.* **1996**, *118*, 5221–5228; d) C. Pataoux, C. Coudret, J. P. Launay, C. Joachim, A. Gourdon, *Inorg. Chem.* **1997**, *36*, 5037–5049; e) J.-P. Sauvage, J.-P. Collin, J.-C. Chambron, S. Guillerez, C. Coudret, *Chem. Rev.* **1994**, *94*, 993–1019; f) N. S. Hush, *Coord. Chem. Rev.* **1985**, *64*, 135–157; g) A. C. Ribou, J. P. Launay, K. Takhashi, T. Nihira, S. Tarutani, C. W. Spangler, *Inorg. Chem.* **1994**, *33*, 1325–1329.

[4] a) C. Creutz, *Prog. Inorg. Chem.* **1983**, *30*, 1–73; b) R. J. Crutchley, *Adv. Inorg. Chem.* **1994**, *41*, 273–325; c) S. Barlow, D. O'Hare, *Chem. Rev.* **1997**, *97*, 637–669; d) N. S. Hush, *Prog. Inorg. Chem.* **1967**, *8*, 391–444.

[5] a) C. Lambert, G. Nöll, J. Schelter, *Nat. Mater.* **2002**, *1*, 69–73; b) P. J. Low, M. A. J. Paterson, H. Puchmann, A. E. Goeta, J. A. K. Howard, C. Lambert, J. C. Cherryman, D. R. Tackley, S. Leeming, B. Brown, *Chem. Eur. J.* **2004**, *10*, 83–91.

[6] W. H. Morrison, S. Krogsrud, D. N. Hendrickson, *Inorg. Chem.* **1973**, *12*, 1998–2004.

[7] a) F. Delgado-Pena, D. R. Talham, D. O. Cowan, *J. Organomet. Chem.* **1983**, *253*, C43–C46; b) M. F. Moore, S. R. Wilson, D. N. Hendrickson, U. T. Mueller-Westerhoff, *Inorg. Chem.* **1984**, *23*, 2918–2920; c) M. F. Moore, S. R. Wilson, M. J. Cohn, T. Y. Dong, U. T. Mueller-Westerhoff, D. N. Hendrickson, *Inorg. Chem.* **1985**, *24*, 4559–4565.

[8] M. Robin, P. Day, *Adv. Inorg. Radiochem.* **1967**, *10*, 247–422.

[9] a) T. Y. Dong, T. J. Ke, S. M. Peng, S. K. Yeh, *Inorg. Chem.* **1989**, *28*, 2103–2106; b) B. Floris, P. Tagliatesta, *J. Chem. Res., Synop.* **1993**, 42–43.

[10] C. Le Vanda, K. Bechgaard, D. O. Covan, *J. Org. Chem.* **1976**, *41*, 2700–2704.

[11] I. Motoyama, M. Watanabe, H. Sano, *Chem. Lett.* **1978**, 513–516.

[12] C. Jutz, *Tetrahedron Lett.* **1959**, 1–4.

[13] a) J. Lukasser, H. Angleitner, H. Schottenberger, H. Kopacka, M. Schweiger, B. Bildstein, K. H. Ongania, K. Wurst, *Organometallics* **1995**, *14*, 5566–5578; b) A. Tárraga, P. Molina, J. L. López, A. Espinosa, D. J. Evans, *Tetrahedron Lett.* **2002**, *43*, 4717–4720.

[14] A. C. Ribou, J. P. Launay, M. L. Sachtleben, H. Li, C. W. Spangler, *Inorg. Chem.* **1996**, *35*, 3735–3740.

[15] B. Bildstein, M. Malaun, H. Kopacka, M. Fontani, P. Zanello, *Inorg. Chim. Acta* **2000**, *300–302*, 16–22.

[16] a) A. G. Osborne, M. W. da Silva, M. B. Hursthouse, K. M. A. Malik, G. Opromolla, P. J. Zanello, *J. Organomet. Chem.* **1996**, *516*, 167–176; b) V. A. Sauro, M. S. Worketin, *Can. J. Chem.* **2002**, *80*, 250–256.

[17] a) A. Tárraga, P. Molina, D. Curiel, M. D. Velasco, *Organometallics* **2001**, *20*, 2145–2152; b) A. Tárraga, P. Molina, D. Curiel, M. D. Velasco, *Tetrahedron Lett.* **2002**, *43*, 8453–8457.

[18] S. K. Davidsen, G. W. Phillips, S. F. Martin, *Org. Synth.* **1993**, *8*, 451–458.

[19] P. Séller, J. D. Dunitz, *Acta Crystallogr., Sect. B* **1982**, *38*, 1741.

[20] J. L. López, A. Tárraga, A. Espinosa, M. D. Velasco, P. Molina, V. Lloveras, J. Vidal-Gancedo, C. Rovira, J. Veciana, D. J. Evans, K. Wurst, *Chem. Eur. J.* **2004**, *10*, 1815–1826.

[21] a) G. L. Geoffroy, M. S. Wrighton, *Organometallic Photochemistry*, Academic Press, New York, **1979**; b) Y. S. Sohn, D. N. Hendrickson, H. B. Gray, *J. Am. Chem. Soc.* **1971**, *93*, 3603–3612.

[22] S. Barlow, H. E. Bunting, C. Ringham, J. C. Green, G. U. Bublitz, S. G. Boxer, J. W. Perry, S. R. Marder, *J. Am. Chem. Soc.* **1999**, *121*, 3715–3723.

[23] N. G. Connelly, W. E. Geiger, *Chem. Rev.* **1996**, *96*, 877–910.

[24] V. Alain, A. Fort, M. Barzoukas, T.-H. Chen, S. R. Blanchard-Desce, S. R. Marder, J. W. Perry, *Inorg. Chim. Acta* **1996**, *242*, 43–49.

[25] M. Masui, H. J. Ohmori, *J. Chem. Soc., Perkin Trans. 2* **1972**, 1882–1887.

[26] a) Y. B. Zu, M. O. Wolff, *Chem. Mater.* **1999**, *11*, 2995–3001; b) Y. B. Zu, D. B. Millet, M. O. Wolf, S. J. Rettig, *Organometallics* **1999**, *18*, 1930–1938.

[27] Y. B. Zu, M. O.Wolf, *J. Am. Chem. Soc.* **2000**, *122*, 10121–10125.

[28] a) I. Yamaguchi, T. Sakano, H. Ishii, K. Osakada, T. Yamamoto, *J. Organomet. Chem.* **1999**, *584*, 213–216; b) M. Horie, T. Sakano, K. Osakada, H. Nakao, *Organometallics* **2004**, *23*, 18–20; c) M. Horie, Y. Suzaki, K. Osakada, *J. Am. Chem. Soc.* **2004**, *126*, 3684–3685.

[29] M. Turki, C. Daniel, S. Zalis, A. Vicek, J. van Slageren, D. J. Stufkens, *J. Am. Chem. Soc.* **2001**, *123*, 11431–11440.

[30] M. C. B. Colbert, J. Lewis, N. J. Long, P. R. Raithby, M. Younus, A. J. P. White, D. J. Williams, N. N. Payne, L. Yellowlees, D. Beljonne, N. Chawdhury, R. H. Friend, *Organometallics* **1998**, *17*, 3034–3043.

[31] Y. Zhu, O. Clot, M. O. Wolf, G. P. A. Yap, *J. Am. Chem. Soc.* **1998**, *120*, 1812–1821.

[32] C. Lambert, G. Nöll, *J. Am. Chem. Soc.* **1999**, *121*, 8434–8442.

[33] a) P. Desjardins, G. P. A. Yap, R. J. Crutchley, *Inorg. Chem.* **1999**, *38*, 5901–5905; b) C. E. B. Evans, M. L. Naklicki, R. J. Crutchley, *Inorg. Chem.* **1995**, *34*, 1350–1354.

[34] T. Ito, N. Imai, T. Yamagushi, T. Hamaguchi, C. H. Londergan, C. P. Kubiak, *Angew. Chem. Int. Ed.* **2004**, *43*, 1376–1381 and references cited therein.

[35] I. R. Gould, D. Noukakis, L. Gómez-Jahn, R. H. Young, J. L. Goodman, S. Farid, *Chem. Phys.* **1993**, *176*, 439–456.

[36] C. Joachim, *Thesis*, Université Paul Sabatier, Tolouse, France, **1990**, pp. 146, 211, and 214.

[37] The proportion of mixed-valence species at half-oxidation (*P*), where $P = K_c^{1/2}/(2 + K_c^{1/2})$ is generally used to compute the intensity of corrected spectra. The comproportionation constant, K_c, which is related to the thermodynamic stability of the mixed-valence compound, of the equilibrium of comproportionation, $[Fe^{II}\text{-L-}F^{II}] + [Fe^{III}\text{-L-}F^{III}] \leftrightharpoons 2[Fe^{II}\text{-L-}F^{III}]$, was calculated for **5f** from the electrochemical data, giving a value of 3.6×10^3. With such a high value of K_c, *P* is almost 100% so that the dependency on K_c is very small and it is not necessary to correct the intensity of the spectrum.

[38] a) E. M. Kober, K. A. Goldsby, D. N. S. Narayane, T. J. Meyer, *J. Am. Chem. Soc.* **1983**, *105*, 4303–4309; b) P. A. Lay, R. H. Magnuson, H. Taube, *Inorg. Chem.* **1988**, *27*, 2364–2371; c) W. M. Laidlaw, R. G. Denning, *J. Chem. Soc., Dalton Trans.* **1994**, 1987–1994.

[39] a) D. E. Richardson, H. Taube, *J. Am. Chem. Soc.* **1983**, *105*, 40–51; b) J. Halpern, L. E. Orgel, *Discuss. Faraday Soc.* **1960**, *29*, 32–41.

[40] According to Hush and Marcus, for symmetrical weakly coupled class II mixed-valence complexes the activation barrier to electron transfer is given by $\Delta G_{MM'}^* = \lambda_{MM'}/4 - V_{MM'} + (V_{MM'}^2/\lambda_{MM'})$; see ref.[41]. With the parameters given in Table 5 for $\mathbf{5f}^{+\cdot}$, a value of $\Delta G_{MM'}^* + \Delta G^\circ_{MM'} = 7.4$ kcal mol^{-1} is obtained for the 4-Fe^{3+} + 1-Fe^{2+} → 4-Fe^{2+} + 1-Fe^{3+} process. The corresponding first-order rate constant (k_{th})can be calculated from $k_{th} = k \cdot \nu_n \cdot \exp(-\Delta G_{MM'}^*/RT)$ where $k = 1$, since the reaction is adiabatic, and the nuclear frequency factor, ν_n, is $2.00 \times 10^{+13}$ s^{-1}, as determined from $\nu_n = [2(V_{MM'})^2/h] \cdot [(\pi^3/\lambda_{MM'}RT)^{1/2}]$. This gives a value for k_{th} of $8.8 \times 10^{+7}$ s^{-1} at 300 K.

 © 2005 Wiley-VCH Verlag GmbH & Co. KGaA, Weinheim

[41] a) R. A. Marcus, *J. Chem. Phys.* **1956**, *24*, 966–978; b) R. A. Marcus, *J. Chem. Phys.* **1965**, *43*, 679; c) R. A. Marcus, N. Sutin, *Inorg. Chem.* **1975**, *14*, 213–216; d) C. Creutz, M. D. Newton, N. Sutin, *J. Photochem. Photobiol. Sect. A* **1994**, *82*, 47–59.
[42] a) E. J. Baerends, D. E. Ellis, P. Ros, *Chem. Phys.* **1973**, *2*, 41–51; b) W. Kohn, A. D. Becke, R. G. Parr, *J. Phys. Chem.* **1996**, *100*, 12974–12980.
[43] a) A. Berces, T. Ziegler, L. Fan, *J. Phys. Chem.* **1994**, *98*, 1584–1595; b) A. Berces, T. Ziegler, *Top. Curr. Chem.* **1996**, *182*, 41–85; c) U. Hohm, D. Goebel, S. Grimme, *Chem. Phys. Lett.* **1997**, *272*, 328–334; d) C. A. Morrison, S. F. Bone, D. W. H. Rankin, H. E. Robertson, F. Parsons, R. A. Coxall, S. Fraser, J. A. S. Howell, P. C. Yates, N. Fey, *Organometallics* **2001**, *20*, 2309–2320.
[44] L. J. Bartolotti, K. Fluchick, in *Reviews in Computational Chemistry* (Eds.: K. B. Lipkowitz, B. D. Boyd), VCH Publishers, New York, **1996**, vol. 7, pp. 187–216.
[45] A. D. Becke, *J. Chem. Phys.* **1993**, *98*, 5648–5652.
[46] C. Lee, W. Yang, R. G. Parr, *Phys. Rev. B* **1988**, *37*, 785–789.
[47] J. W. McIver, A. K. Komornicki, *J. Am. Chem. Soc.* **1972**, *94*, 2625–2633.
[48] Gaussian 98, Revision A.9, M. J. Frisch, G. W. Trucks, H. B. Schlegel, G. E. Scuseria, M. A. Robb, J. R. Cheeseman, V. G. Zakrzewski, J. A. Montgomery Jr., R. E. Stratmann, J. C. Burant, S. Dapprich, J. M. Millam, A. D. Daniels, K. N. Kudin, M. C. Strain, O. Farkas, J. Tomasi, V. Barone, M. Cossi, R. Cammi, B. Mennucci, C. Pomelli, C. Adamo, S. Clifford, J. Ochterski, G. A. Petersson, P. Y. Ayala, Q. Cui, K. Morokuma, D. K. Malick, A. D. Rabuck, K. Raghavachari, J. B. Foresman, J. Cioslowski, J. V. Ortiz, A. G. Baboul, B. B. Stefanov, G. Liu, A. Liashenko, P. Piskorz, I. Komaromi, R. Gomperts, R. L. Martin, D. J. Fox, T. Keith, M. A. Al-Laham, C. Y. Peng, A. Nanayakkara, M. Challacombe, P. M. W. Gill, B. Johnson, W. Chen, M. W. Wong, J. L. Andres, C. Gonzalez, M. Head-Gordon, E. S. Replogle, J. A. Pople, Gaussian, Inc., Pittsburgh PA, **1998**.
[49] R. Gleiter, R. Seeger, *Helv. Chim. Acta* **1971**, *54*, 1217–1220..
Received: November 30, 2004

 © 2005 Wiley-VCH Verlag GmbH & Co. KGaA, Weinheim